Mechanical and thermophysical properties of cement mortars including bio-based microencapsulated phase change materials

Franck Komi Gbekou [a,*], Karim Benzarti [a,*], Abderrahim Boudenne [b], Anissa Eddhahak [c], Myriam Duc [d]

[a] Univ Gustave Eiffel, Ecole des Ponts, CNRS, Navier, F-77447 Marne-la-Vallée, France
[b] Univ Paris-Est Créteil, CERTES, F-94010 Créteil, France
[c] Arts et Métiers ParisTech, Laboratoire Procédés et Ingénierie en Mécanique et Matériaux (PIMM), F-75013 Paris, France
[d] Univ Gustave Eiffel, GERS-SRO, F-77447 Marne-la-Vallée, France

ARTICLE INFO

Keywords:
Bio-based
Microencapsulated phase change materials (mPCMs)
Liquid dispersion
Cement mortar
Thermophysical properties
Mechanical strength
Microstructure

ABSTRACT

This study investigates the mechanical and thermophysical performance of cement mortars incorporating microencapsulated phase change materials (mPCMs), which consist of an aqueous dispersion of 100% bio-based fine core–shell particles. A specific protocol was used to manufacture the mortar samples, which ensures a homogeneous particle distribution and prevents microcapsule leakage. The addition of mPCMs to the mortar causes both a decrease in density, an increase in porosity, and a substantial loss of mechanical strength. Conversely, hot-disk characterization revealed a large improvement in the thermal performance. The system containing 8 wt% mPCMs exhibits a good balance between its mechanical and thermal properties.

1. Introduction

In 2020, the building and construction sector was responsible for ~36 % of the global energy consumption and ~37 % of CO_2 emissions, according the International Energy Agency (IEA) [1,2]. The energy demand from buildings has continued to increase over the last few years, mainly driven by the easy access to energy services in developing countries and the growing use of energy-consuming devices for temperature regulation in cold/hot regions. Therefore, improving the energy efficiency of buildings is crucial in the current context of global climate change.

Energy consumption in the building industry includes both the "embodied energy" consumed during the manufacturing process/transport of building materials and the construction or demolition phase, as well as the "operational energy" related to the building's operations and use (air conditioning, heating and lighting, domestic equipment, etc.) [3]. Although the impact of embodied-energy consumption has recently received increasing attention from architects and engineers, most technical developments still focus on reducing end-user consumption. To date, various solutions have been deployed in the field based on passive or active energy management methods, such as the use of insulation panels, lighting management systems, and automatic control systems used for air conditioning/heating installations [4–7].

Recently, researchers have also developed thermal energy storage (TES) systems, which are considered to be a very promising approach [8–12]. These systems store a certain quantity of energy that can then be released at a later stage to meet a specific need. Several TES technologies are readily available based on chemical heat storage (by forming/breaking chemical bonds), sensible heat storage (by heating/cooling a material), and latent heat storage (by melting/solidifying a material).

According to the literature, latent heat thermal energy storage (LHTES) based on the use of phase change materials (PCMs) has been considered the most attractive approach in the context of building applications because it allows the storage of large amounts of energy [11,13–15]. The operating principle of PCMs relies on their ability to change their physical state over a narrow temperature range; when the temperature increases above the melting temperature, the PCMs pass from their solid to liquid state, absorb thermal energy from the environment, and store this energy in the form of latent heat. When the temperature decreases, the material can undergo a reversible transition from the liquid to solid state and release the stored energy. This capability of PCMs to absorb or release energy can be advantageously used to mitigate temperature variations in the indoor environment of buildings with the aim of improving the thermal comfort of the occupants and

* Corresponding authors.
E-mail addresses: komi.gbekou@univ-eiffel.fr (F.K. Gbekou), karim.benzarti@univ-eiffel.fr (K. Benzarti).

reducing energy consumption [12,13].

Regardless of whether they are organic (most often derived from hydrocarbons), inorganic (salt hydrates or metallic compounds), or based on eutectic mixtures, PCMs can be easily incorporated into conventional construction materials (such as plaster, concrete, and mortar) to produce construction components with enhanced thermal storage properties, such as wallboards, floors, and roofs [13–15]. In practice, different methods can be used to introduce PCMs into building materials, including their direct incorporation and the use of macro- or microencapsulated PCMs. Microencapsulation has gained a lot of research interest over the last decade and consists of packing the PCM material into spherical core–shell capsules with diameters ranging from <1 μm to ~500 μm [14]. The outer shell is usually composed of a high-molecular-weight polymer, which acts as a barrier to prevent leakage of the PCM core and its interactions with the components present in the host building material.

Microencapsulated PCMs (mPCMs) can be produced in the form of either a dry powder or liquid dispersion. However, powders are conventionally used for building applications; they are generally introduced into cement-based materials at the end of the mixing process using a low rotational speed to prevent any possible damage to the PCM capsules [16]. Conversely, the use of liquid mPCM dispersions is poorly documented in the literature and to the best of our knowledge, very few studies have explored this approach [13,17]. Snoeck *et al.* reported the difficulties in incorporating these liquid products into cement mortars using the same mixing protocol utilized for powders due to their viscous/sticky texture [17]. Consequently, the distribution of PCM capsules in the hardened mortar is very heterogeneous. Therefore, alternative fabrication methods should be developed to improve the microstructure of these materials.

Another interesting feature is the recent availability of bio-based mPCMs [18,19]. These eco-friendly systems are composed of fatty esters or natural waxes derived from renewable vegetal resources. They present several advantages over their petroleum-based counterparts, such as a reduced carbon footprint, good biodegradability, and low flammability. However, their incorporation into building materials has not been explored to date.

Several studies have investigated the possibility of enhancing the thermal performance of cement composites (i.e., mortar or concrete) upon introducing mPCM powders based on petroleum-based paraffin waxes. For example, Lecompte *et al.* evaluated the thermal conductivity of cement mortars and concretes with various mPCM contents using the guarded hot-plate method [20]. Measurements were conducted at temperatures below and above the melting range (20.5 and 30.5 °C, respectively), at which paraffin is in the solid and liquid state, respectively. Under both conditions, the authors observed a decrease in the thermal conductivity as a function of the mPCM, which was well fitted with the Maxwell model, assuming the random distribution of the spherical mPCM particles in a homogeneous medium. Furthermore, at a given mPCM content, the thermal conductivities of the mortar/concrete samples were significantly higher at 30.5 °C (liquid state) when compared to those observed at 20.5 °C (solid state). Similarly, Jayalath *et al.* determined the thermal conductivity and thermal resistivity of concrete samples containing various amounts of mPCMs using two experimental techniques (needle probe and C-therm methods). Measurements were conducted at 35 °C, at which the paraffin component of the mPCMs was in its liquid state. Both the thermal conductivity and diffusivity of concrete were found to decrease with the mPCM content (for example, a 45 % reduction in the thermal conductivity was observed upon the introduction of 5 wt% mPCMs). This trend was attributed to (i) the low conductivity of the organic mPCMs and (ii) the amount of air entrapped in the concrete during the incorporation of the mPCM powder, which increases the overall porosity and hence affects the thermal properties (heat transfer by conduction is partially replaced by natural convection). Cao *et al.* observed the same decrease in the thermal conductivity and an increase in the latent heat (both determined using the guarded hot plate method) when introducing mPCMs to Portland cement concrete [21]. According to the authors, these effects observed on the material scale are also beneficial in terms of energy saving in buildings because the power consumption for stabilizing the indoor temperature at 23 °C may be reduced by up to 11 % after adding only 3.2 wt% mPCMs to the concrete envelope. Similarly, Hunger *et al.* highlighted a reduction in the thermal conductivity and an increase in the thermal mass of self-compacting concrete upon the incorporation of mPCM powder [22]. They also reported that the energy needed to maintain the indoor temperature at 23.5 °C was reduced by 12 % in the case of a concrete wall containing 5 wt% mPCMs when compared to a plain concrete wall. In summary, most studies suggest a significant improvement in the thermal performance of cement composites will be achieved upon the addition of mPCMs.

Nevertheless, the introduction of foreign particles alters the microstructure of concrete, and its mechanical properties will be affected. Numerous studies have highlighted a significant decrease in the mechanical strength is observed following the addition of mPCMs to concrete. For instance, Fenollera *et al.* observed a reduction in the compressive strength of ~7 % for every 5 wt% of mPCMs added (with respect to the quantity of cement in the mixture) [13]. Similarly, Djamai *et al.* and Lecompte *et al.* reported decreases in the compressive strength of 34.1 and 50 % for mortar containing 5 and 6.3 wt% mPCMs, respectively (with respect to the total mass of the mix in this case) [20,23]. According to most authors, the observed loss in the mechanical strength can be attributed to several reasons: (i) PCM microcapsules exhibit very low mechanical strength and act as voids or defects in concrete; (ii) the overall porosity of the cement composite increases with the mPCM content, as previously mentioned, which impacts both the density and mechanical properties of the material; (iii) some of the PCM capsules may be damaged during the mixing process and the leaked paraffin wax may hinder or interact with the hydration process of the cement matrix [24].

In this context, an optimal mPCM content should be determined to achieve a compromise between the enhancement in the thermophysical properties and loss of mechanical strength, depending on the target application of the concrete or mortar material.

The main objective of the present study was to investigate the thermophysical and mechanical properties of cement mortars formulated using different amounts of a bio-based liquid mPCM dispersion (denoted PCM mortars), as previous knowledge on this specific type of material is very limited. The effects of the mPCM content on the microstructure of PCM mortars were also investigated to better understand the evolution trends observed in the macroscopic properties.

In the first part of this study, the experimental methods and mortar design are presented in detail and a specific protocol is developed to add the liquid mPCM dispersion into the fresh mortar mix, which allows control over the overall content of PCM microcapsules and a constant workability of the PCM mortars to be maintained. The second part of the study is dedicated to our experimental results. After a preliminary characterization of the liquid mPCM dispersion in terms of its particle size distribution and thermal properties of the microcapsules, a comprehensive test program was conducted on mortar samples containing different dosages of the PCM microcapsules, up to 13.6 wt% (equivalent to ~24.3 vol%) with respect to the total composition. Microstructural investigations were conducted on these mortars using scanning electron microscopy and thermogravimetric analysis to evaluate the effect of adding mPCM on the porous structure and hydrate composition. The mechanical and thermophysical properties of the PCM mortars were then assessed, and their evolution as a function of the

Table 1
Composition of the reference cement mortar (M0) based on reference [28].

Component	*Sand*	*OPC*	*CSA*	*SP*	*Water*
Dosage (g)	800	627.75	47.25	1.76	236.25

mPCM dosage were analyzed in light of the microstructural aspects mentioned beforehand.

2. Materials and methods

2.1. Raw materials

A commercial product known as CrodaTherm™ ME29D, which is manufactured by Croda International (Snaith, UK), was selected as the PCM in this study and was denoted as ME29D. This product was prepared in the form of a liquid dispersion of the microencapsulated particles in water with a solid content of 50 wt%. The dispersed particles consist of an organic PCM core derived from plant-based feedstocks surrounded by an acrylic polymer shell. The mass ratio between the PCM core and polymer shell was ~92/8 [25]. The ME29D technical datasheet reports melting and crystallization peak temperatures of 28.8 and 23.5 °C, respectively, as well as heats of melting and crystallization of 183 and − 179 kJ kg^{-1}, respectively (determined using differential scanning calorimetry (DSC) at a scanning rate of 1 °C min^{-1})[26]. This liquid mPCM dispersion presents several interesting features in the framework of this study. It can be easily incorporated into hydraulic binder formulations (i.e., cement mortars) at an early stage of the mixing process. In addition, ME29D is certified 100 % bio-based and formaldehyde free, which ensures both a reduced environmental footprint and low safety/health hazards.

An existing formulation from the literature [27,28] was selected as the reference cement mortar sample used in this study, which was initially developed for additive manufacturing applications. This choice was mainly guided by another aspect of our research, which explores the 3D printability of mortars containing PCM additives (this has not been addressed in the present paper). The original composition of this reference mortar, denoted M0, is detailed in Table 1 and based on a water-to-cement (W/C) ratio of 0.35.

In this formulation, two types of cement were combined at a ratio of 93/7 wt%: Ordinary Portland Cement containing 99 % clinker (EXTREMAT® CEM I 52,5N-SR3 SEG), denoted OPC, and a rapid setting Sulfo-aluminous cement (Alpenat R^2) denoted CSA, which are both manufactured by VICAT company (L'Isle-d'Abeau, France). The small amount of CSA included in the mix affects the rheology of the fresh mortar at an early age and acts as a setting accelerator, which promotes the buildability of the mortar in 3D printing applications [26,27].

To ensure the good workability of the mortar, a polyvalent acrylic copolymer superplasticizer/high water reducer (VISCOCRETE TEMPO 11) obtained from SIKA Company (Baar, Switzerland), denoted as SP, was also used. The SP product has a solid content of 30 % according to its technical datasheet. Siliceous sand complying with the EN 196-1 standard [29] (graded sand with a maximum grain size of 2 mm and moisture content <0.2 %) was supplied by Société Nouvelle du Littoral (Leucate, France).

2.2. Mix design and preparation of the PCM mortar samples

Different specimens were fabricated for our experimental study, including samples of the reference cement mortar (M0) and mortars containing various contents of the mPCM particles. The compositions of all of the mortars studied are summarized in Table 2. The amounts of mineral components (sand, OPC, and CSA) and SP were kept unchanged in the various mixes, and the only components varied were the quantities of mPCM particles and water added. Because only full bags of standard sand were used for the preparation of the mortar mixes, the quantities of all of the other components were given per bag of sand (mass = 1350 g). In addition, the composition of the reference mortar (M0) was strictly identical to that of the original mortar reported in Table 1, but the quantities were expressed for one bag of sand.

Each mortar composition was identified using the designation Mx, where × corresponds to the target dosage of solid mPCM particles originating from the liquid dispersion and incorporated into the mortar mix, expressed as the weight percentage of the M0 reference sample (i.e., the mass of solid mPCM particles divided by the total mass of all M0 components × 100). The target solid mPCM dosage was varied in the range of 0–20 wt%. The actual weight fraction of the mPCM particles in the fresh mortar mix (i.e., the ratio between the mass of the solid mPCM particles and the total mass of all components expressed in wt.%) is also displayed in Table 2, as well as the volume fraction of the mPCM particles calculated considering the densities of the various component materials in the fresh mix (a density of 870 kg m^{-3} was assumed for the solid mPCM particles, in accordance with the manufacturer's data). Notably, the highest volume fraction of mPCMs considered in this work was ~25 % (for the M20 mortar mix), which is rather high when compared with most PCM mortars studied in the literature.

The total amount of water in the mix corresponds to the quantity of water originating from the liquid ME29D dispersion and the additional amount of water added during the mixing process. The latter was adjusted so that the workability of the mortar mix (spread diameter provided by the slump test) remains the same as that of the M0 reference mortar The procedure for adjusting the amount of water mixed is described in detail below. The resulting W/C ratios are also reported in Table 2, as well as the percentage evolution compared with the M0 reference sample (the value in brackets in the W/C column). This percentage evolution of the W/C ratio can also be defined as the water demand of the mPCMs used in the mortar formulations, as proposed by Sanfelix *et al.* [30].

$$\text{Water demand compared to the M0 reference mortar (in \%)} = \left(\frac{(W/C)_{Mx}}{(W/C)_{M0}} - 1\right) \times 100 \quad (1)$$

where $(W/C)_{M0}$ is the water-to-cement ratio of the M0 reference mortar and $(W/C)_{Mx}$ is the water-to-cement ratio of the PCM mortar of composition Mx.

Notably, the quantity of water originating from SP was not taken into account in the total amount of water reported in Table 2 because this quantity is limited and the SP content was not varied in this study (the mass ratio between SP and cement was kept constant at 0.26 % for all of the mortar formulations studied, i.e. the same ratio as that used in the M0 reference mortar [27,28]).

Table 2
Compositions of the various PCM mortar admixtures.

Designation	Sand (g)	OPC (g)	CSA (g)	SP (g)	Mass of solid mPCM particles (g)	Total amount of water (g)	W/C ratio	Mass fraction of mPCM particles (wt.%)	Volume fraction of mPCM particles (vol.%)
M0	1350	1059.33	79.73	2.96	–	398.67	0.35	0	0
M5	1350	1059.33	79.73	2.96	144.53	537.88	0.47 (+34 %)	4.55	10.53
M10	1350	1059.33	79.73	2.96	289.07	851.36	0.75 (+114 %)	7.96	16.16
M15	1350	1059.33	79.73	2.96	433.06	1006.23	0.88 (+151 %)	11.03	20.94
M20	1350	1059.33	79.73	2.96	578.14	1190.72	1.05 (+200 %)	13.57	24.35

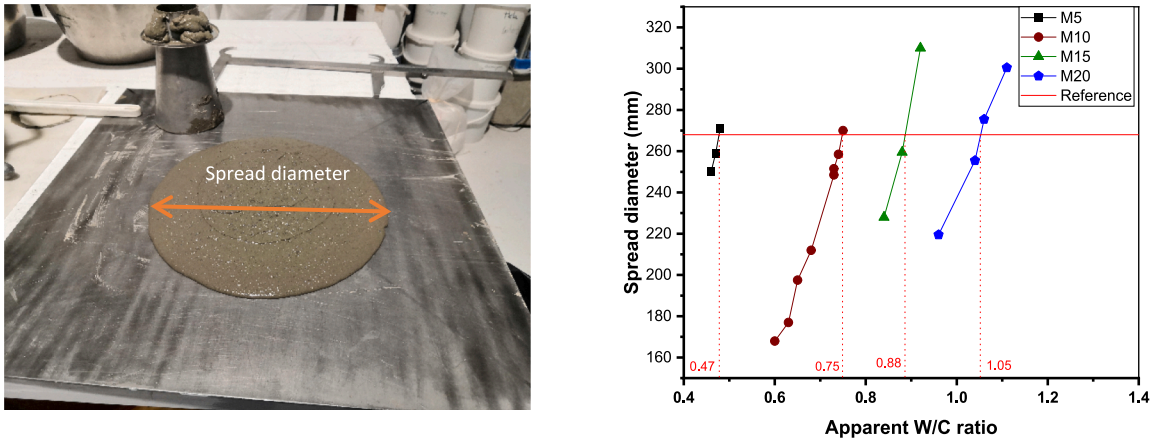

Fig. 1. Optimization of the water dosage using mini-slump tests: (a) Experimental setup and (b) evolution curves of the spread diameter as function of the W/C ratio obtained for the various PCM mortar admixtures studied.

To provide the reader with a comprehensive set of data, the densities of the various component materials and theoretical compositions of the mortars expressed in kg m^{-3} for the fresh mix are also provided in the Appendix.

In practice, a programmable mortar mixer (model E092N from Matest Spa Company, Treviolo, Italy), is used to prepare the different mortar samples. The mixing protocol strictly followed the specifications of the EN 196-1 standard for conventional mortars in terms of the rotational speed and duration of the mixing sequence.

In the case of the M0 reference mortar, the different steps used in the mixing procedure were as follows: **(1)** A mixture of the two cements (OPC and CSA in the proportion of 97/3 wt%) was placed in the mixer tank. Water containing the SP was then added to the cement, and the zero time was counted from the moment the water came into contact with the cement. **(2)** Mixing was started at a low speed and sand was added slowly during the first minute while mixing at low speed (140 rotations per minute). The mortar was then mixed at a high speed (285 rpm) for 30 s. **(3)** The rotation was stopped for 30 s to scrape the mortar from the bottom of the tank. **(4)** Another high-speed mixing was performed for 2.5 min.

The same protocol was used for the PCM mortars with the only difference being that the ME29D liquid dispersion was added together with the mixing water in the first step. In this case, the amount of liquid dispersion to be added was directly determined by the target content of solid mPCM particles in the mortar, whereas the complementary amount of mixing water was adjusted so that the workability of the fresh PCM mortar mix remained the same as that of the M0 reference mortar.

In practice, different water dosages are considered for each PCM mortar composition studied, and slump tests were performed using an Abrams mini cone to determine the resulting spread diameter (Fig. 1a). The evolution curves of the spread diameter as a function of the apparent W/C ratio (where W corresponds to the total amount of water, including both water originating from the ME29D dispersion and mixing water) were then plotted for the various PCM mortar compositions, as shown in Fig. 1b. These curves allow the optimum W/C ratios (and hence deduce the adequate amount of mixing water) required to achieve the same spread as that of the M0 reference mortar (i.e., 268 mm, represented by the horizontal red line in Fig. 1b) to be graphically determined. The optimal W/C ratios are listed in Table 2.

In general, the water demand in the mix increased significantly with the mPCM content. This result is consistent with the literature and may be attributed to the absorption of water by the hydrophilic acrylic shell of the mPCM particles [5,10] and possibly the alteration of the granular distribution in the PCM mortar admixtures.

Immediately after mixing, the various mortar admixtures were cast into metallic molds to prepare parallelepiped samples with dimensions of 4 × 4 × 16 cm^3 for mechanical characterization, as well as 4 × 4 × 8 cm^3 samples for thermal and microstructural characterization. The molds were filled into two layers, and each layer was subjected to 52 blows (for ~1 min) using a shock table. After casting, the samples were covered and stored for 24 h at 20 ± 1 °C. After 24 h, the samples were demolded, hermetically wrapped with plastic film, and finally conditioned at 20 ± 1 °C until characterization at 28 d.

2.3. *Characterization techniques*

2.3.1. *Laser diffraction analysis*

The size distribution of the mPCM particles in the ME29D dispersion was determined using wet-laser diffraction. Tests were performed using a MASTERSIZER 3000E analyzer (Malvern Panalytical, Malvern, UK) equipped with a liquid dispersion unit operated at a rotation rate of 800 rpm. The liquid mPCM dispersion was first diluted in water to reduce the particle concentration and facilitate light diffusion induced by the penetration of the laser beam into the medium. Generally, this method enables the particle size distribution to be determined in the range of 0.1–1000 μm.

2.3.2. *Differential scanning calorimetry (DSC)*

The thermal properties of the mPCM particles were determined using DSC on a DSC 250 apparatus (TA Instruments, New Castle, DE, USA). Solid samples of the aggregated mPCM particles were initially prepared by drying a volume of liquid ME29D dispersion in an oven at 60 °C for at least 48 h until a compact solid material was obtained (denoted as solid mPCM material). Small amounts (15 mg) of this material were used for characterization.

DSC analyses were conducted in temperature modulation mode (MDSC) according to the protocol detailed in the ASTM E2716-09 standard [31]. This method enables one to measure the specific heat capacity (Cp) of the sample with good accuracy (up to ±2 %), which is generally better when compared to conventional DSC [32]. During the same experiment, the characteristics of the melting and crystallization peaks of the solid mPCM material during the heating and cooling phases were also evaluated.

In practice, a preliminary Cp calibration of the calorimeter is achieved over a temperature ranging from –20 to 60 °C using a sapphire standard. A low scanning rate of 0.5 °C/min was used for this calibration and the subsequent analyses to ensure thermal equilibrium conditions were obtained within each sample [33], and the temperature

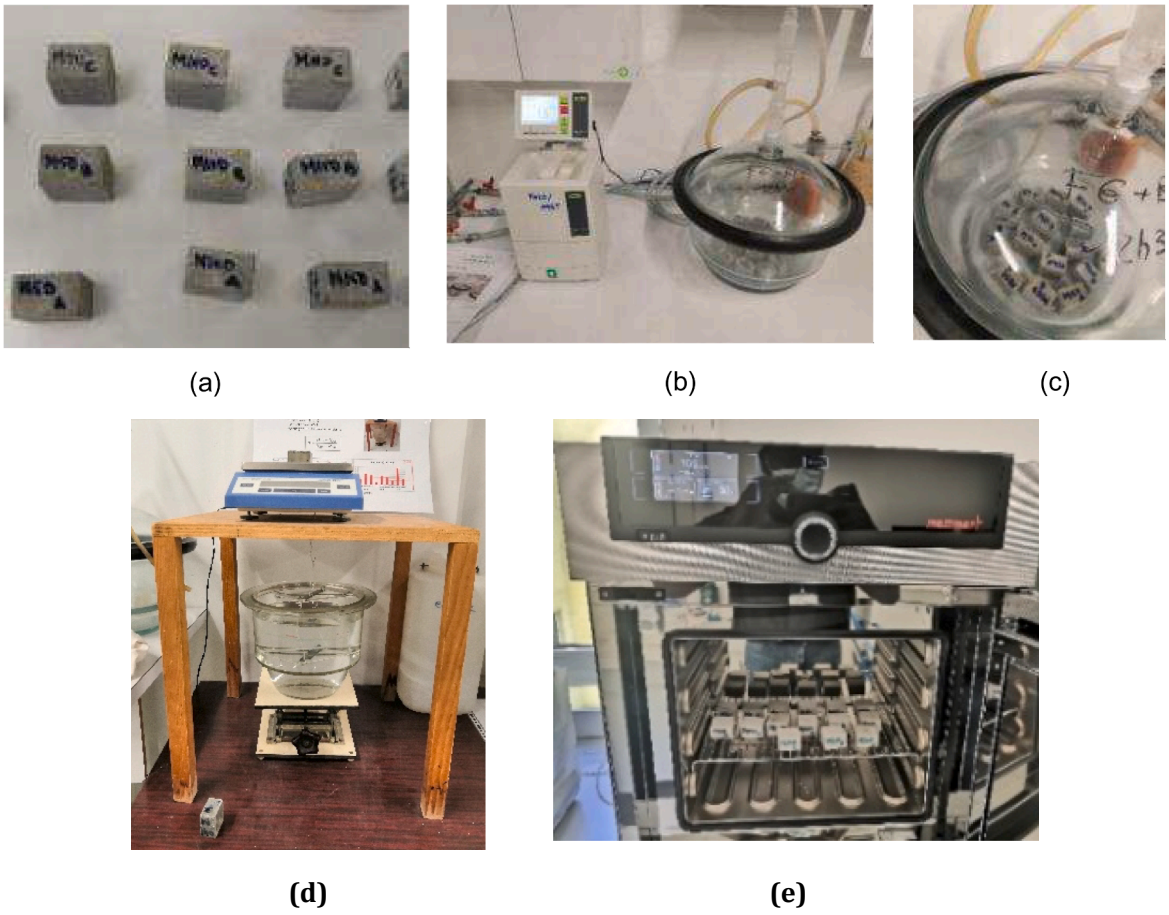

Fig. 2. Experimental protocol used to determine the water accessible porosity and apparent density based on the NF P 18-459 standard: (a) 2 × 2 × 4 cm^3 mortar samples, (b) conditioning under vacuum, (c) imbibition with water, (d) hydrostatic weighing, and (e) drying in an oven at 105 °C.

modulation was set at ±1 °C with a period of 120 s, as advised by the manufacturer's instructions provided with the DSC apparatus [34].

Each sample of solid mPCM material was then subjected to 2 successive heating/cooling cycles in the temperature range from –20 to 60 °C under the same scanning conditions as those used for the calibration. The characteristics of the melting peak (onset, melting point, and latent heat) were assessed from the heat flow thermogram recorded during the second heating step, whereas the characteristics of the crystallization peak were determined during the second cooling step. Further, the Cp values of the mPCM particles in the solid and liquid states were determined during the second heating step and were taken as the reversing heat capacity values measured at 10 and 50 °C, respectively (these two temperatures are located below and above the melting transition of the phase change material). Four samples were analyzed to calculate the mean value and standard deviation of these properties.

2.3.3. Water accessible porosity and apparent density of hardened PCM mortars

Both the water-accessible porosity and apparent density of the PCM mortars were determined in accordance with the NF P18-459 standard [35]. The experimental protocol was comprised different steps, as summarized in Fig. 2. Specimens with dimensions of 4 × 4 × 8 cm^3 were first cut into smaller samples (2 × 2 × 4 cm^3), placed in a desiccator under vacuum for 4 h, and then imbibed in water for 72 h until saturated. At this stage, the water-saturated samples were weighed in air and water using a hydrostatic balance system. The same specimens were then conditioned in an oven at 105 °C and their mass loss was monitored every day until it was stabilized, which made it possible to determine their dry mass. Finally, the water-accessible porosity (ε in %) and apparent density (ρ_d in kg m^{-3}) were calculated using the following expressions:

$$\varepsilon\ (\%) = \frac{Ms_{air} - M_{dry}}{Ms_{air} - Ms_{water}} \times 100 \quad (2)$$

$$\rho_d = \frac{M_{dry}}{Ms_{air} - Ms_{water}} \times \rho_{water} \quad (3)$$

where Ms_{air} and Ms_{water} are the mass of the water-saturated sample measured in air and water (g), respectively; M_{dry} is the mass of the dry sample (g); and ρ_{water} is the density of water (kg m^{-3}).

For each mortar composition, the mean values and standard deviations were determined from three samples.

2.3.4. Microstructural observations using scanning electron microscopy (SEM)

SEM characterization was performed using a QUANTA 400 microscope (FEI Company, Hillsboro, OR, USA) operated at an electron voltage of 20 kV under low vacuum. Qualitative observations were conducted on the ME29D dispersion after the evaporation of water to visualize the size of the mPCM particles. The fractured surfaces of the samples of the different PCM mortars aged for 28 d were also observed. To obtain the fractured surfaces, mortar samples with dimensions of 4 × 4 × 8 cm^3 were broken into small pieces using a hammer. The surfaces did not undergo any metallization or specific treatment prior to the SEM observations.

SEM images were collected in both secondary electron (SE) and backscattered electron (BSE) mode, the former providing information on the topography of the analyzed surface and the latter providing a contrast based on the chemical composition.

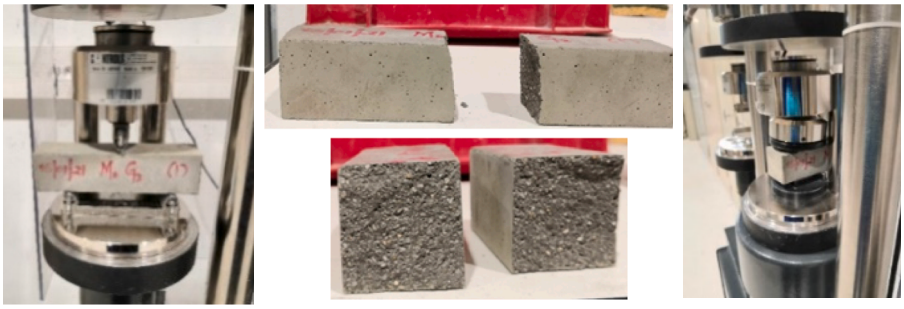

(a) (b) (c)

Fig. 3. Mechanical characterization of the PCM mortars: (a) 3-point bending test, (b) fractured mortar samples after the bending test, and (c) compression test on the half specimens.

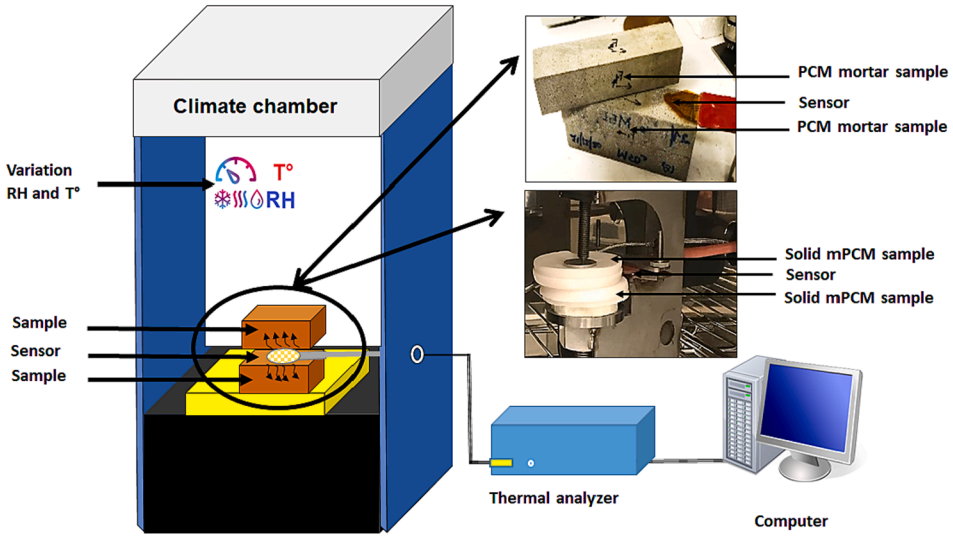

Fig. 4. Schematic representation of the hot disk setup used to measure the thermophysical properties of the solid mPCM samples and PCM mortars under controlled temperature and RH conditions.

2.3.5. Thermogravimetric analysis (TGA)

TGA was also performed on samples of the solid mPCM material (obtained by the evaporation of water from the liquid ME29D dispersion) and on the fine powders of the various PCM mortars (obtained by grinding a small amount of the mortar samples and sieving the resulting powder below 315 μm). The mass loss was monitored while applying a temperature ramp to the samples to identify the degradation point of the organic/mineral components and hence, collect information on the structure and composition of the analyzed materials. Simultaneous thermal differential analysis (STDA) was also performed on the same sample to facilitate the detection of decomposition phenomena specific to the organic components, which can be identified as exothermic peaks in the STDA curves.

The experiments were performed using an STA 409 apparatus (NETZSCH Company, Selb, Germany). The protocol involved increasing the temperature from 25 to 1250 °C at a heating rate of 10 °C min^{-1} an under an air environment (80 mL min^{-1}). Three tests were conducted for each sample.

2.3.6. Mechanical characterization of the hardened PCM mortars

The mechanical properties of the hardened PCM mortars were assessed after 28 d, according to the EN 196-1 standard [29] using a Pilot Pro press from Controls S.p.a. (Milano, Italy) with a load capacity of 300 kN.

In the first step, 3-point bending tests were performed on the samples with dimensions of 4 × 4 × 16 cm^3 (six specimens per mortar sample) to determine the flexural strength, as shown in Fig. 3a. After breakage, the 12 half specimens were retrieved and subjected to compression tests to evaluate their compressive strength (Fig. 3b and c).

2.3.7. Characterization of the thermophysical properties

The thermophysical properties of the solid mPCM material (solid disks with diameters of 68 mm and thickness of ~5 mm obtained by drying fixed volumes of the ME29D dispersion in aluminum cups), and the various PCM mortars (with dimensions of 4 × 4 × 8 cm^3) were determined using the hot disk (HD) method. A TPS 2500 S device from the Hot Disk Company (Gothenburg, Sweden) comprising a sensor connected to a thermal constant analyzer was used. The sensor was a "Kapton insulated" model (ref 5501) from Hot Disk® and had a radius of 6.4 mm.

The HD technique relies on the theory of a transient plane source, as specified by the ISO 22007-2 standard [36]. It uses a sensor element in the shape of a double spiral, which is placed between two samples of the same material (solid mPCM or mortar specimens) and can be considered infinite in all directions with respect to the sensor. The latter acts as both as a heat source to increase the temperature of the sample and as a "resistance thermometer'' to record the time-dependent increase in temperature. Such a device (Fig. 4) enables the simultaneous rapid, accurate, and nondestructive evaluation of the thermal conductivity (λin W m^{-1} K^{-1}), thermal diffusivity (α in m^2 s^{-1}), and volumetric heat capacity of the sample ($\rho.C_p$ in J m^{-3} K^{-1}).

The thermophysical properties of porous building materials can be

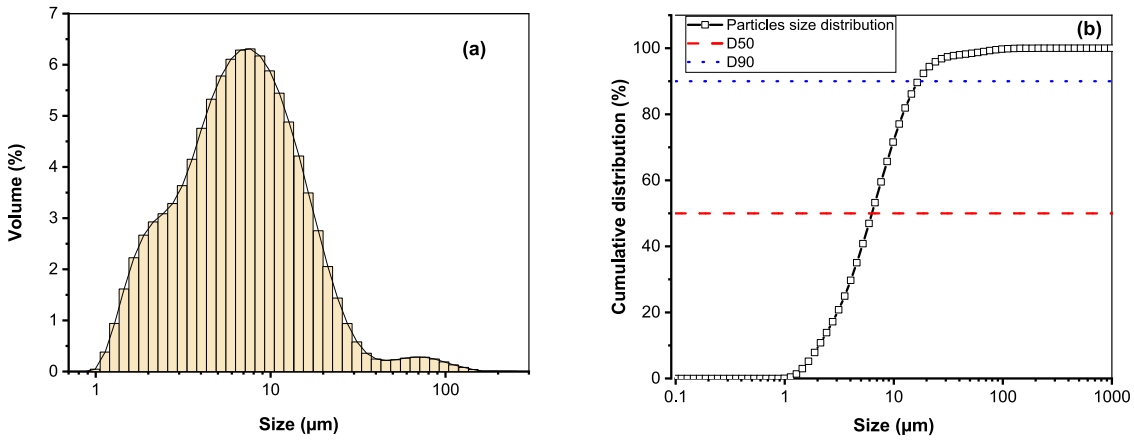

Fig. 5. Particle size distribution of the ME29D dispersion as determined by wet laser diffraction analysis: Particle size distribution curves by (a) volume and (b) cumulated volume.

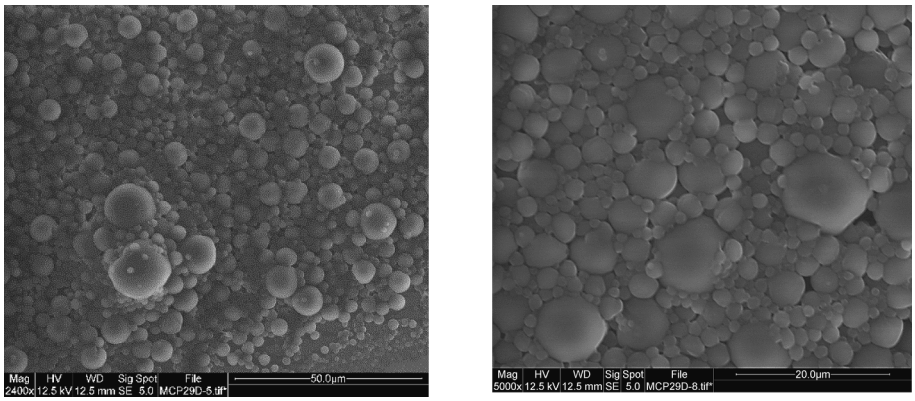

Fig. 6. SEM images obtained at different magnifications of the microencapsulated PCM particles contained in the ME29D dispersion (after the evaporation of water).

dependent on several factors, such as the temperature and moisture content of the sample. Therefore, it is important to perform the measurements in a controlled environment. In our case, the samples were preliminary conditioned for at least one week at 20 °C and 50 % RH in a climate chamber to reach an equilibrium state prior to characterization. Subsequently, the entire experimental setup (sensor placed between the two samples) was placed in the climate chamber to control both the temperature and RH conditions during the measurements (Fig. 4).

Furthermore, the mPCMs have a melting point of ~29 °C and consequently, the thermophysical properties of PCM mortars may be affected by phase change phenomenon over a large range of temperature around this transition point. Therefore, HD measurements were performed over a large temperature range from 10 to 50 °C. Further, a constant 50 % RH was used in the climate chamber to prevent any variation in the moisture content of the samples during the measurements.

Finally, for a given experimental configuration (i.e., a given type of material and fixed temperature and RH conditions), the manufacturer of the HD instrument recommends determining the thermal properties (λ, α, and, $\rho.C_p$) of the analyzed sample from a single measurement and specified that the accuracy and reproducibility of this measurement are better than 5 and 1 %, respectively (as evaluated from a series of repeated tests on standard materials) [37]. In the present study, single measurements were performed in the case of the solid mPCM sample and a maximum level of uncertainty of 5 % was considered in accordance with the manufacturer's specifications. The experimental values of the PCM mortars were averaged over three repeated measurements, and the uncertainties were based on the calculated standard deviations. Overall, it was found that they were below the uncertainty level of 5 % claimed by the manufacturer.

3. Results and discussion

3.1. Preliminary characterization of the mPCM dispersion

A preliminary characterization of the ME29D dispersion was performed to assess the particle size distribution and thermal properties of the microencapsulated PCM particles. This first set of experiments was considered necessary because most studies in the literature focus on the incorporation of dry mPCM powder systems in cement mortars, whereas the characteristics of liquid mPCM dispersions are much less documented.

3.1.1. Particle size distribution

Fig. 5 shows the particle size distribution of mPCM in the ME29D dispersion, as determined by wet laser diffraction analysis. The distribution curve according to volume (Fig. 5a) shows that the dispersion was mainly composed of fine particles with sizes <10 μm (the maximum volume percentage was observed for a particle size of ~7 μm). However, one can also observe a small amount of larger-sized particles with diameters of up to 100 μm.

The cumulative distribution curve (Fig. 5b) shows that the median particle size (D50) is 6.7 μm, and 90 % of the particles have diameters of <16.4 μm (D90). These features demonstrate that the ME29D dispersion was mainly composed of fine mPCM particles. This may influence the incorporation of mPCMs into cement mortar because it may affect the microstructure of the system.

Fig. 6 shows the SEM images of the ME29D dispersion after evaporation of the water content. These observations confirm the previous results regarding the particle size distribution and show that the mPCM particles exhibit a spherical shape. In addition, some agglomerated

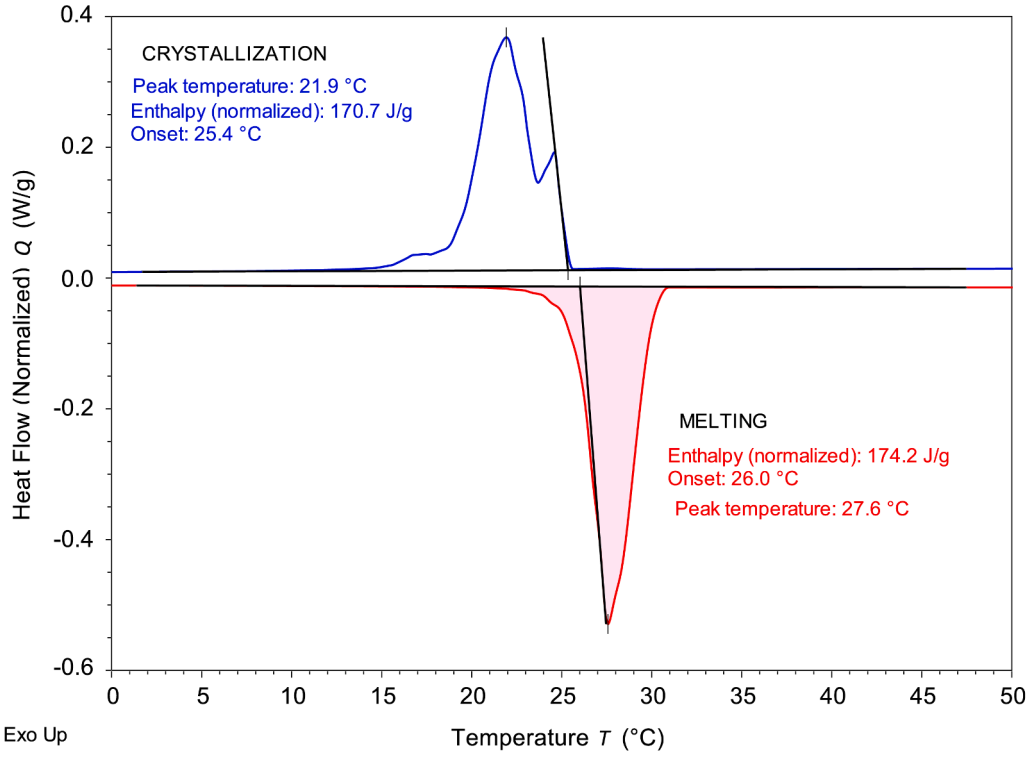

Fig. 7. Typical DSC thermograms (heat flow *versus* temperature) obtained over the heating/cooling steps at a rate of 0.5 °C min^{-1} for the mPCM particles (after evaporation of water from the ME29D dispersion).

Table 3
Characteristics of the melting and crystallization peaks of the mPCM particles, as determined by DSC at a rate of 0.5 °C min^{-1}.

Properties		Mean value	Standard deviation
Characteristics of the melting peak	Latent heat of melting (J/g)	172.5	2.7
	Onset (°C)	26.0	0.2
	Peak maximum (°C)	27.8	0.2
Characteristics of the crystallization peak	Latent heat of crystallization (J/g)	169.1	2.4
	Onset (°C)	25.3	0.1
	Peak maximum (°C)	21.8	0.2

particles were detected, which were probably formed via coalescence during the evaporation of water from the analyzed sample.

3.1.2. *DSC characterization of the mPCM particles*

The solid mPCM material was analyzed using DSC (see protocol in Section 2.3.2). Fig. 7 presents the typical heat flow thermograms collected during the heating/cooling steps, which display the melting and crystallization peaks of the mPCM particles. The characteristics of these peaks (averaged over four repeated tests) are listed in Table 3.

The melting and crystallization points were observed at ~28 and ~22 °C, respectively, and the latent heats of melting/crystallization were ~172 and 169 J g^{-1}. These values were consistent with the manufacturer's data [26]. Further, one can notice that the overall temperature range covered by both the melting and crystallization transformations of the PCM compound was rather large (between 12 and 31 °C). This confirms that the thermal properties of the mPCM particles vary significantly in this domain and justified the fact that HD measurements on PCM mortars should be conducted over a large temperature range.

Fig. 8 shows the typical reversing heat capacity as a function of temperature for the mPCM particles obtained at a heating rate of 0.5 °C min^{-1}. From this thermogram, the specific heat capacities (C_p) of the mPCMs in the solid and liquid phases could be determined. The latter were identified at temperatures of 10 and 50 °C, respectively (these temperatures were arbitrarily chosen below and above the temperature range covered by both the crystallization/melting peaks). The average values obtained upon four repeated tests were $C_{p-sol} = 1.63 \pm 0.13$ J g^{-1} °C^{-1} in the solid phase at 10 °C and $C_{p-liq} = 2.05 \pm 0.15$ J g^{-1} °C^{-1} in the liquid phase at 50 °C. These values are very similar to those reported in the literature for pure paraffin waxes, such as nonadecane [38].

Complementary TGA was conducted to evaluate the degradation behavior of the mPCM particles at high temperature (see protocol in section 2.3.5). Fig. 9 shows the evolution of the sample mass *versus* temperature, as well as the DTG and SDTA curves. Different events were detected in these curves.

- The first weight loss (and hence the first degradation) began at ~210 °C, which was consistent the flash point reported in the datasheet of the CrodaTherm ME29 product.
- The weight loss in the range of 210–260 °C (also characterized by shoulder 1 in both the DTG and SDTA curves) may be attributed to the decomposition of the acrylic shell of the mPCM particles.
- The most important weight loss was observed in the range of 260–400 °C, which was related to the decomposition of the bio-based PCM core of the particles. This degradation was also reflected by the large exothermic peak observed in the SDTA curve. Furthermore, two separate peaks were visible in the DTG curve in this temperature range (peak 2 at 312 °C and peak 3 at 360 °C), suggesting that the core PCM material is a two-component mixture.
- Finally, a slight weight loss was observed between 410 and 520 °C (associated with peak 4 in both the DTG and SDTA curves), which

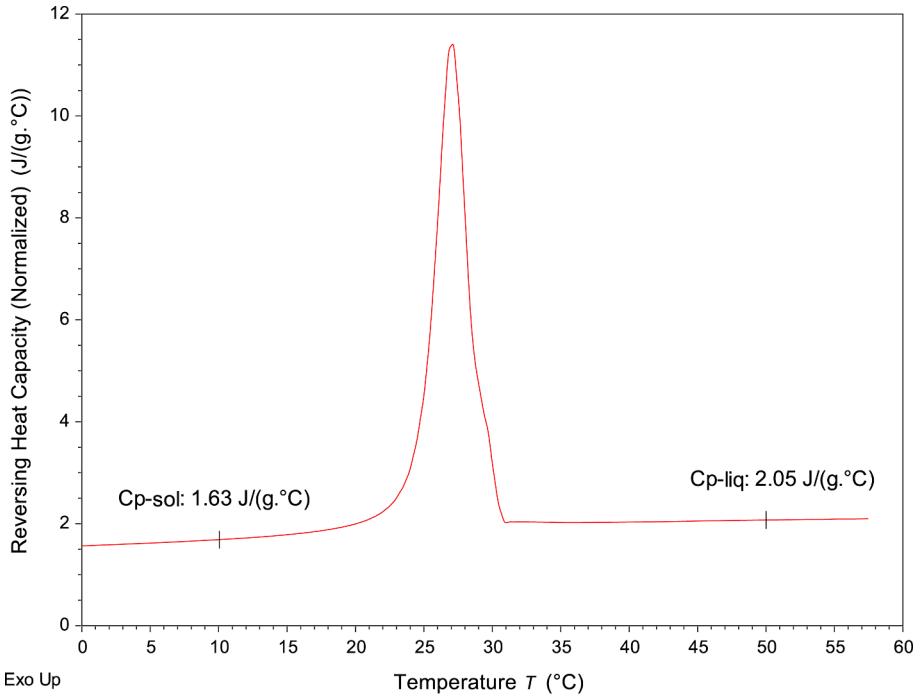

Fig. 8. Typical thermogram (reversing heat capacity *versus* temperature) of the mPCM particles (after evaporation of water from the ME29D dispersion) obtained at a scanning rate of 0.5 °C min^{-1}.

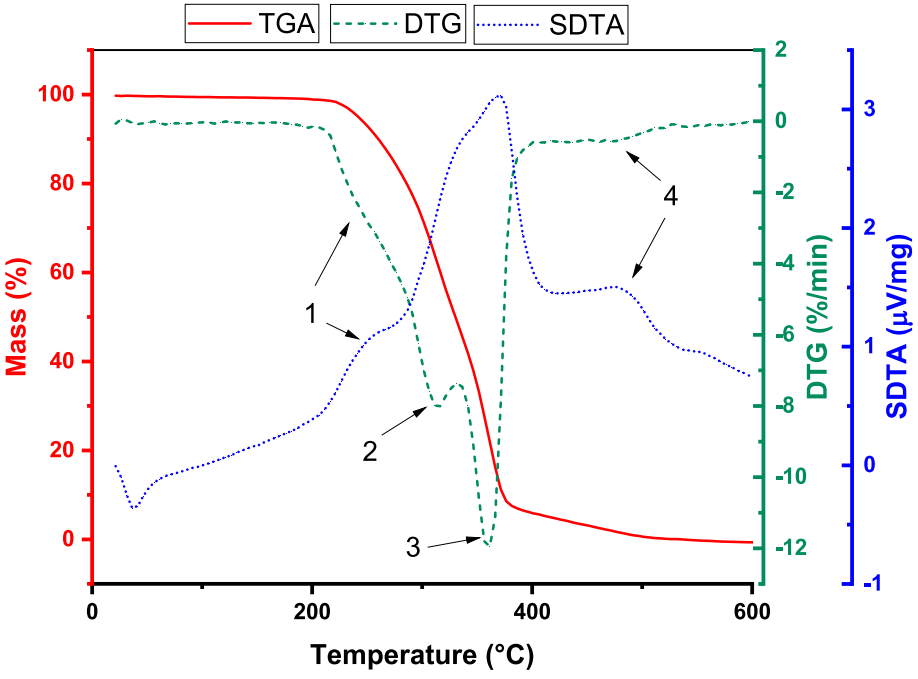

Fig. 9. Typical TGA, DTG, and STDA curves recorded at 10 °C min^{-1} under an air atmosphere for the mPCM particles (after evaporation of water from the ME29D dispersion).

may be attributed to the degradation of the additives used in the microencapsulation process, such as the surfactant used to stabilize the oil/water emulsion [15] and highly cross-linked phase in the polymer shell [39].

3.1.3. *Thermophysical properties of the microencapsulated PCMs*

The thermophysical properties of the solid mPCM material were determined using the HD technique (see Section 2.3.7.) at 50 % RH and over a temperature range from 5 to 50 °C to cover the entire phase change domain.

Fig. 10 shows the evolution of the thermal conductivity (λ) and thermal diffusivity (α) as a function of temperature. The error bars correspond to an uncertainty of 5 % in the experimental data, as stated by the manufacturer of the HD instrument.

For both properties, the experimental values initially appear to linearly decrease when the temperature was increased from 5 to 15 °C, at which the PCM core was in its solid state. A sharp decrease was then observed in the temperature range between 15 and 30 °C, at which the

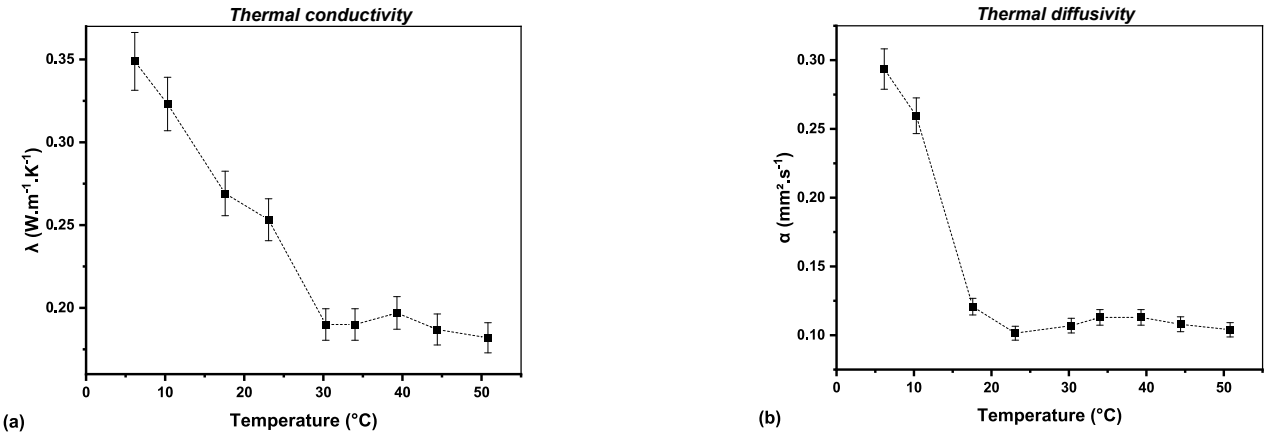

Fig. 10. Evolution curves of the (a) thermal conductivity and (b) thermal diffusivity obtained for the mPCM particles as a function of temperature.

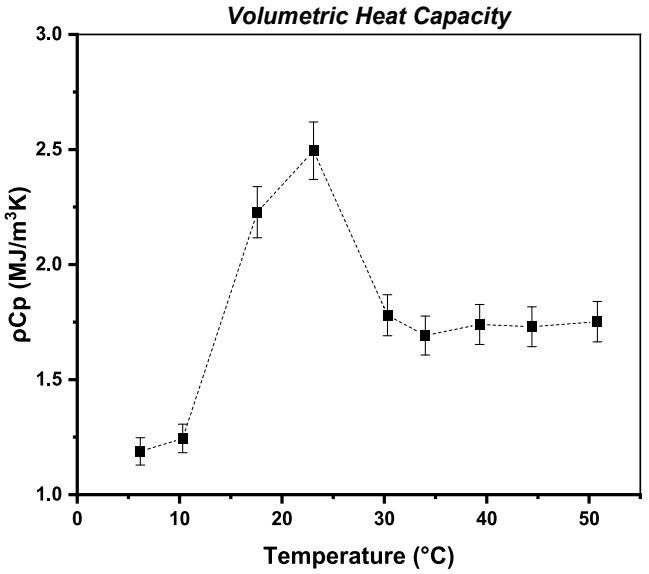

Fig. 11. Evolution of the volumetric heat capacity of the mPCM particles with temperature.

solid–liquid transition of the PCM core occurred. Notably, the system was not at equilibrium in this temperature range; hence, the experimental values provide a general trend but should be considered with caution. Finally, both the thermal conductivity and diffusivity were almost constant in the liquid phase at temperatures between 30 and 50 °C.

These overall trends are similar to those observed in the literature for pure paraffin wax [38,40]. The thermal conductivities measured in the solid state (0.25–0.35 W m^{-1} K^{-1}) and liquid state (~0.19 W m^{-1} K^{-1}) were also consistent with the typical data reported for paraffin wax. The sharp decrease in the thermal conductivity and diffusivity observed near the melting temperature can be attributed to the change in the density of the PCM core, which is a typical first-order phase transition [41].

Fig. 11 shows the evolution of the volumetric heat capacity ($\rho.C_p$) as a function of temperature for the mPCM particles. A peak was observed in the temperature range of 15–30 °C, relating to the melting transition of the PCM core. Furthermore, $\rho.C_p$ appears to stabilize in the liquid state (above 35 °C), which was ~ 40 % higher than those obtained in the solid state (at 10 °C).

Finally, the specific heat capacity (C_p) of the material in the solid/liquid state can be estimated by considering that the density of the mPCM particles was 870 kg m^{-3}, as reported by the manufacturer. The values were determined to be 1.43 and 2.02 J g^{-1} °C^{-1} at 10 and 50 °C, respectively, which were of the same order of magnitude as the C_{p-sol} and C_{p-liq} values previously measured using DSC.

3.2. Experimental investigations on PCM mortars

This section is dedicated to our experimental investigations on PCM mortars. A characterization study was first conducted to assess the effect of the mPCM content on the microstructure of the hardened mortars (i.e., the distribution of the mPCM particles in the volume of the specimens, the integrity of the mPCM particles, and induced porosity). The mechanical properties of the PCM mortars were then determined and analyzed in light of the previous microstructural aspects. In the last stage, the thermal properties of the various mortars were collected using the HD technique with the aim of identifying a PCM mortar composition suitable for building applications that combines both enhanced energetic performance and a limited drop in its mechanical properties.

3.2.1. Microstructural characterization

3.2.1.1. SEM observations. Fig. 12 presents the SEM images collected in backscattered electron mode (BSE), which display the microstructure of the different PCM mortar samples. The images obtained at three different magnifications (×600, ×1200, and ×5000) are provided for each type of material.

For the M0 reference mortar (Fig. 12a to a"), one can observe a compact microstructure with a limited apparent porosity. Due to the chemical contrast offered by the BSE images, a few light gray inclusions were detected, which correspond to anhydrous cement grains. This suggests that the hydration reaction was still incomplete after curing for 28 d.

The microstructures of the mortars becomes much more porous upon the addition of the mPCM particles, which was consistent with many studies reported in the literature [20,42]. With increasing PCM content, the SEM images reveal a growing density of small cavities uniformly distributed in the material. Most of these cavities are filled with individual mPCM particles (appearing in black due to the chemical contrast in the BSE images), whereas some other cavities only contain occluded air. This increased porosity results from both the excess water added to control the workability of the fresh mortar mixes and the air entrapped during the incorporation of the mPCM particles.

At higher magnification (i.e., Fig. 12c" and e"), it was also observed that the mPCM particles in the mortar samples still exhibit a regular spherical shape, suggesting that they were not significantly damaged during the mixing/sample casting process and that the integrity of the acrylic shell was preserved.

These observations confirm that the protocol adopted for the fabrication of the mortar specimens, in which the liquid mPCM dispersion

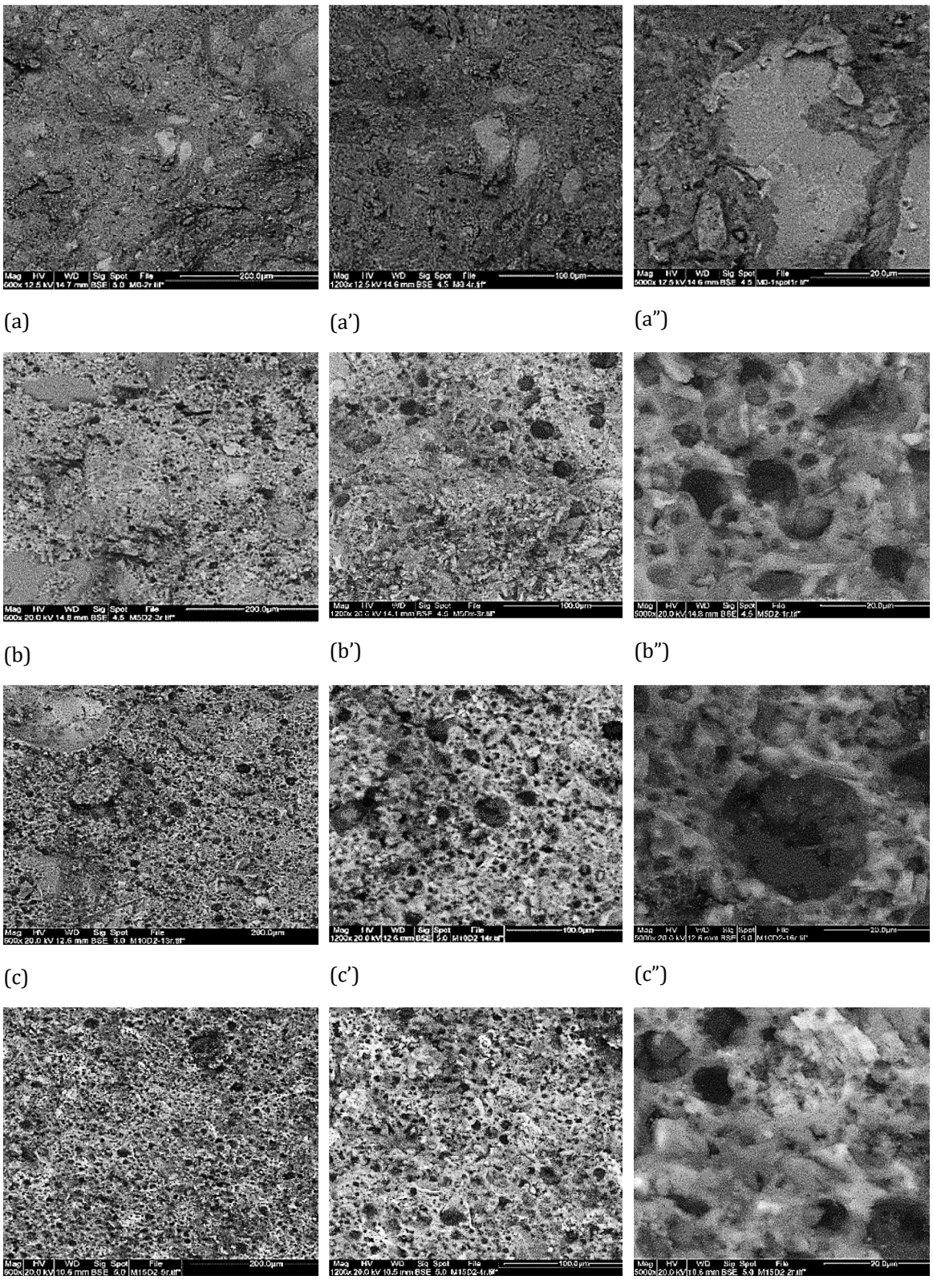

Fig. 12. SEM images obtained in BSE mode showing the microstructure of the various PCM mortars at different magnifications: (a) to (a") M0, (b) to (b") M5, (c) to (c") M10, (d) to (d") M15, and (e) to (e") M20.

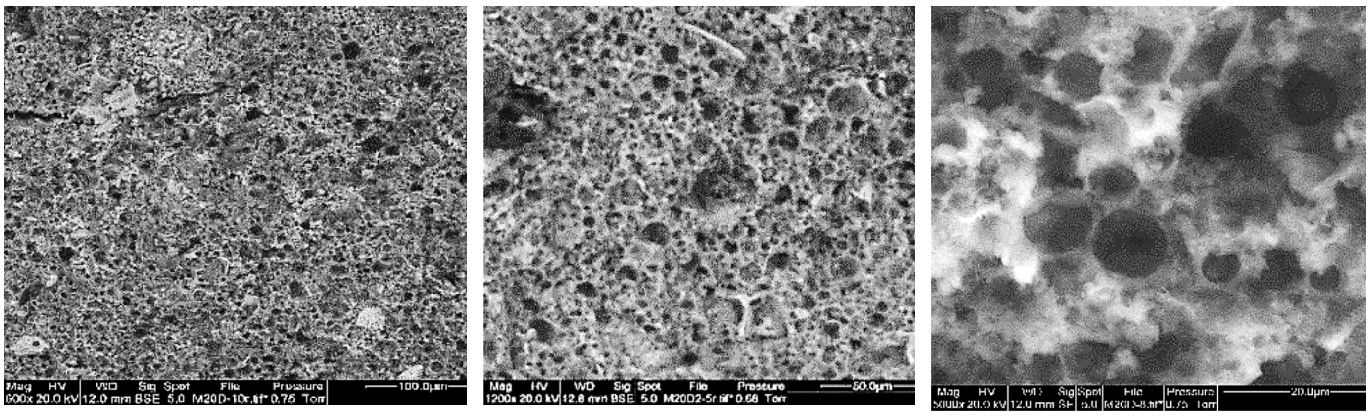

(e) (e') (e")

Fig. 12. (*continued*).

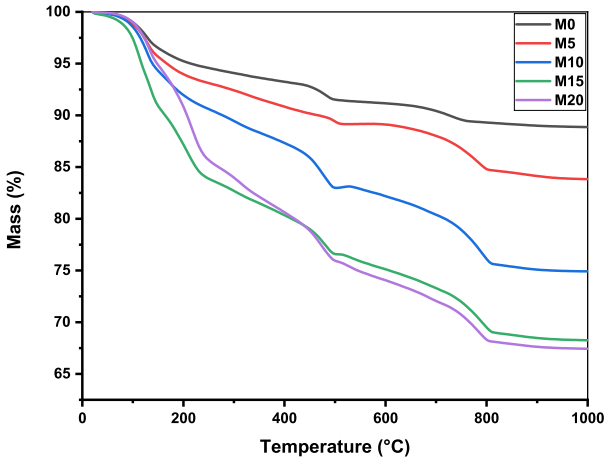

Fig. 13. Typical TGA curves collected at a heating rate of 10 °C min^{-1} for the various PCM mortars studied.

was added at an early stage in the mixing process, enables the formation of mortar microstructures with uniformly distributed and globally intact mPCM particles. This is a significant improvement over the mixing protocol used by Snoeck *et al.* [17], in which the liquid PCM dispersion was introduced at a later stage and resulted in a very heterogeneous microstructure. It is also worth noting that liquid dispersions of mPCM particles with thicker acrylic shells are currently under development (for instance, by Croda Company), which should further increase the resistance of the microcapsules against mechanical deterioration during the mixing phase.

3.2.1.2. Thermogravimetric analysis (TGA). TGA was also conducted on the hardened PCM mortar samples after 28 d, according to the protocol detailed in Section 2.3.5.

Fig. 13 shows the typical evolution of the sample mass after heating at 10 °C min^{-1}, while Fig. 14 displays the DTG curves. These curves reveal several degradation phases that are dependent on the mortar composition.

Regarding the M0 reference mortar, three distinct phases were detected, which are characteristic of the products formed by the hydration reactions between the OPC/CSA cements and water [15,17,20]:

- The first weight loss step was observed in the temperature range of 30 to 130 °C (associated with peak A in the DTG curve). This was attributed to the evaporation of capillary free water and the loss of water bound to the ettringite hydrates.
- The weight loss between 130 and 400 °C was attributed to the loss of water bound to the hydrated calcium silicates (CSH). In particular, shoulder B observed in the DTG curve between 160 and 240 °C was related to the dehydration of calcium monocarboaluminate (AFm).
- The mass loss in the range of 400–540 °C and peak C observed in the DTG curve correspond to the dehydroxylation of the calcium hydroxide phase (portlandite $Ca(OH)_2$).
- Finally, the weight loss between 600 and 800 °C (and peak D in the DTG curve) results from the decarbonation of calcium carbonate.

In regard the PCM mortars, the following remarks can be made:

- The TGA curves show that the total weight loss at 900 °C was significantly higher than that of the M0 reference mortar and that this gap increases with the mPCM content. The higher mass loss can be attributed to the degradation of mPCM particles and the excess water added during sample fabrication used to maintain the level of the workability (see section 2.2), which remains bound to the cement hydrates.
- The DTG curves of the PCM mortars show the same degradation peaks previously observed for the M0 reference mortar, and hence, the same cement hydrates were present (ettringite, AFm, portlandite, calcium carbonate). Notably, that the amplitude of peak D was much higher than that observed for the M0 sample, suggesting the presence of a higher amount of calcium carbonate. This effect may result from the higher porosity (as evidenced by SEM), which makes the PCM mortars more vulnerable to carbonation [24].
- The DTG curves indicate the presence of two new peaks that were not detected in the M0 reference mortar (peak 1 at 210 °C and peak 2 at 360 °C, Fig. 14). A comparison with the DTG curve obtained for the mPCM particles (dotted line) shows that these peaks correspond to the decomposition of the acrylic shell and PCM core of the microcapsules, respectively, as previously discussed in Section 3.1.2.
- The situation is more complex in the temperature range of 400–550 °C, where the PCM mortars exhibit higher weight losses when compared to the M0 reference sample (Fig. 13). The shape and amplitude of the DTG peak C were also significantly altered in the

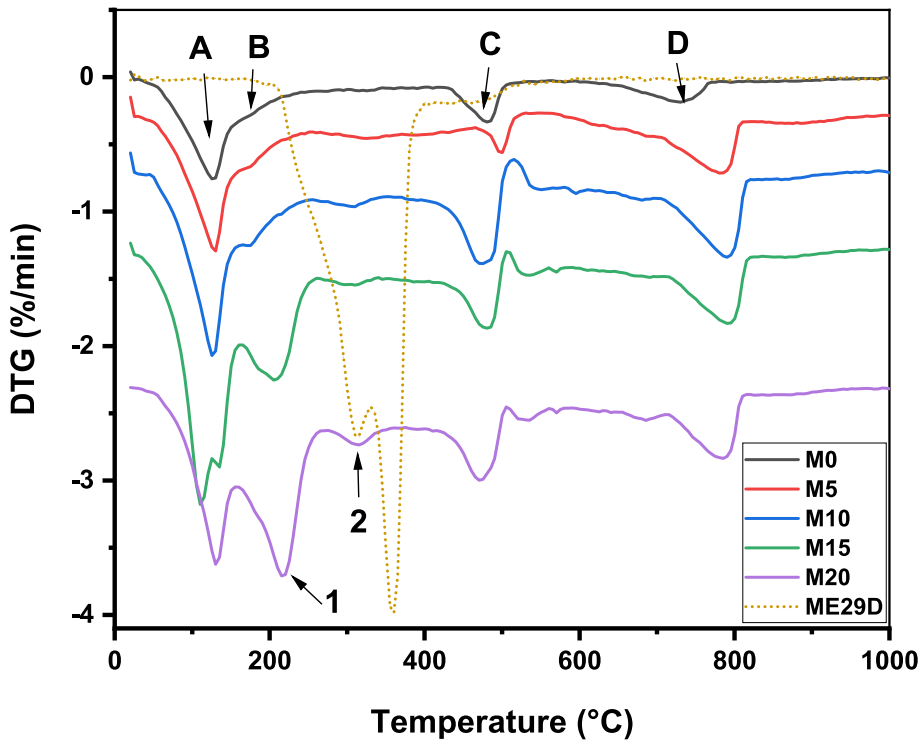

Fig. 14. Typical DTG curves (first derivative signals) obtained for the various PCM mortars. The DTG curve obtained for the mPCM particles is superimposed for comparison (dotted curve, labelled ME29D).

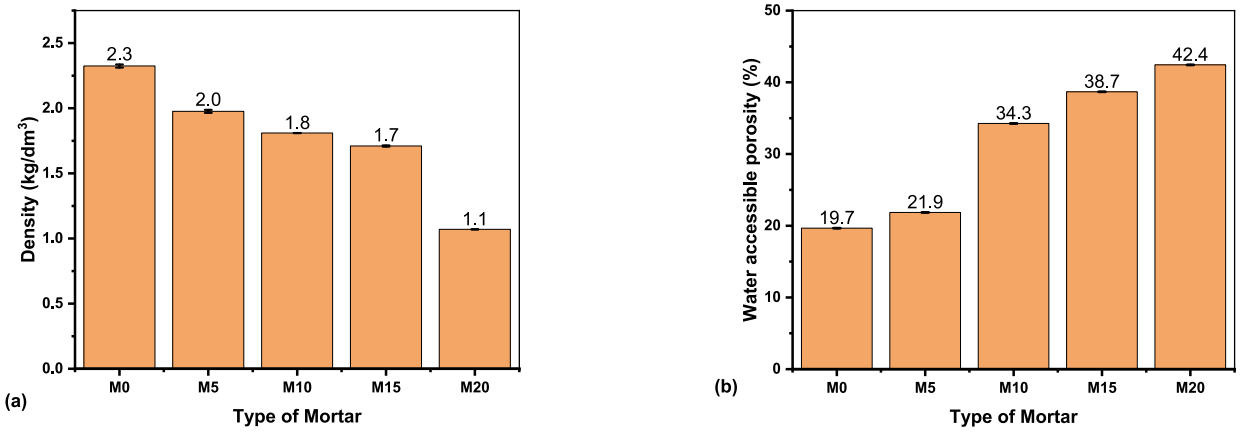

Fig. 15. Mean values of the (a) apparent density and (b) water accessible porosity of the various PCM mortar compositions according to the NF P18-459 standard.

PCM mortars (Fig. 14), indicating that this peak incorporates both the dehydroxylation of portlandite and the decomposition of an organic component in the mPCM particles (most likely the surfactant or a cross-linked component of the shell, as discussed in Section 3.1.2). In addition, several authors have suggested that mPCM particles interfere with the hydration process of PCM mortars, which may explain the TGA/DTG results observed in this temperature range. Aguayo *et al.* reported that small mPCM particles (micron size) act as nucleation sites for the formation of portlandite and become surrounded by a hydrate layer [39]. Sharma *et al.* reported that the higher mass loss of PCM mortars in the range 400–550 °C may also result from a physical cross-linking process between the paraffin wax that leaked from some damaged microcapsules and portlandite [43], but the breakage/leakage of the mPCM particles was not confirmed by SEM in the present work. Further analysis of the percentage of the hydration products was not possible because of the overlap of the portlandite hydroxylation and mPCM decomposition processes on the TGA curves. Complementary investigations may be conducted using X-ray diffraction (XRD) to obtain more information regarding the quantification of cement hydrates, but this is beyond the scope of the present paper.

3.2.1.3. Apparent density and water accessible porosity. Fig. 15a and 15b provide the mean values of the apparent density and water accessible porosity obtained for the various PCM mortars according to the NF P18-459 standard (see the protocol in section 2.3.3). These experimental data were also plotted as a function of the effective volume content of the mPCMs, as shown in Fig. 16.

The apparent density of the mortars decreases as the volume content of the mPCMs increases. This evolution shows a linear trend for mPCM contents in the range of 0–20 vol%, whereas a sharper drop in the density was observed at higher dosages.

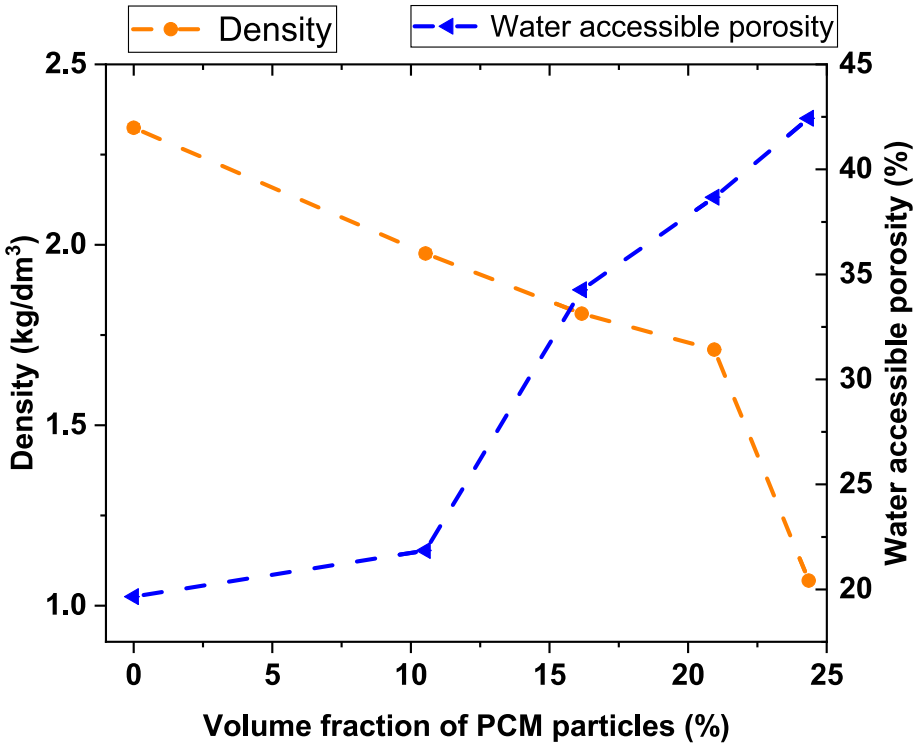

Fig. 16. Evolution of the apparent density and water accessible porosity of the PCM mortars as a function of the volume fraction of the mPCM particles.

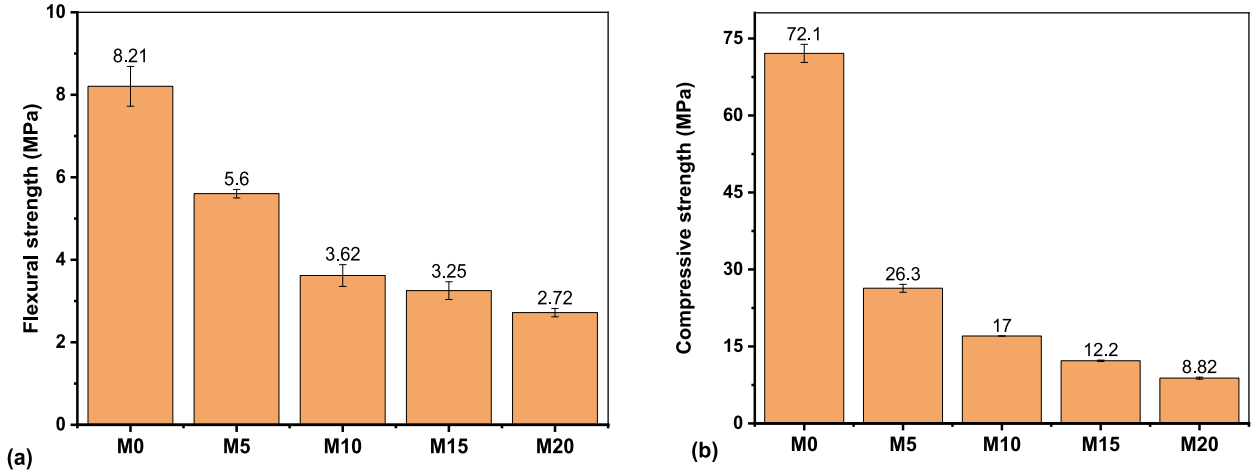

Fig. 17. Mechanical properties of the various PCM mortars: The mean values of the (a) flexural and (b) compressive strength.

In addition, a substantial increase in the water-accessible porosity of the mortars was observed with the mPCM content, especially at dosages > 10 vol%. This result was consistent with the increase in porosity previously confirmed using SEM (Section 3.2.1.1) and was in agreement with the density evolution. This was also consistent with the hydrate composition of the mortars determined using TGA; higher quantities of calcium carbonate were detected at high mPCM dosages, which may be related to the increased porosity of the PCM mortars that favors the carbonation process.

Similar results have been reported in the literature. For instance, Fenollera *et al.* reported a decrease in the density of mortar of ~ 1.1 % for every 5 wt% of PCM added [13]. Cunha *et al.* found that the incorporation of 20 % PCM (by mass of cement) results in a ~ 16 % decrease in the mortar density [44]. Such an evolution of density can be assigned to multiple factors [21,22]:

- mPCM particles have a lower density than other mineral components in the mortar. As some of these constituents are replaced, the overall density of the mortar decreases.
- The introduction of mPCMs also alters the granular distribution of the mortar and hence, modifies the packing density.
- The porosity of the PCM mortars increases with the mPCM content, which also contributes to the decrease in density. This increased porosity results from the air entrapped during the incorporation of the mPCM particles and the excess water added to control the workability of the fresh mortar mix.

3.2.1.4. Mechanical properties. Fig. 17 provides the mean values of the flexural and compressive strengths obtained for the various PCM mortars after 28 d based on a series of 6 and 12 repeated tests, respectively (see experimental protocol in Section 2.3.6). The error bars derived from the standard deviations are also displayed. Fig. 18 shows the

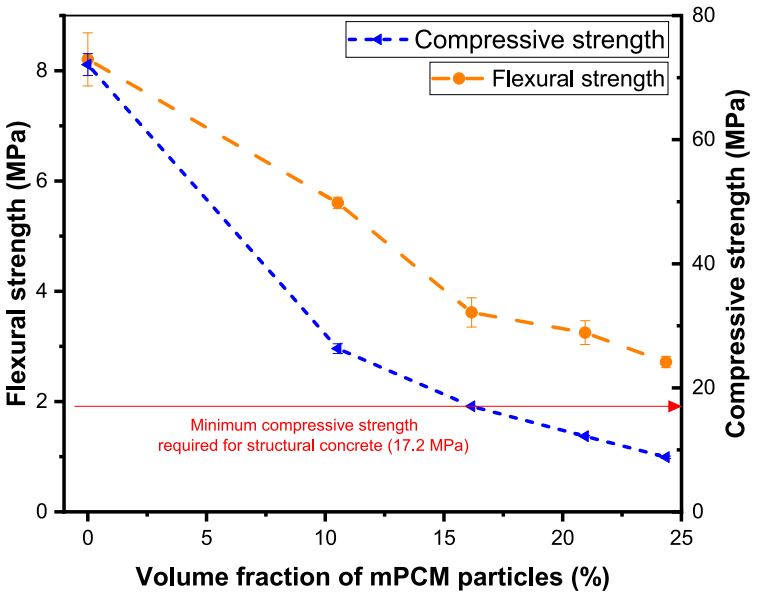

Fig. 18. Evolution of the flexural and compressive strength of the PCM mortars as a function of the volume fraction of mPCM particles.

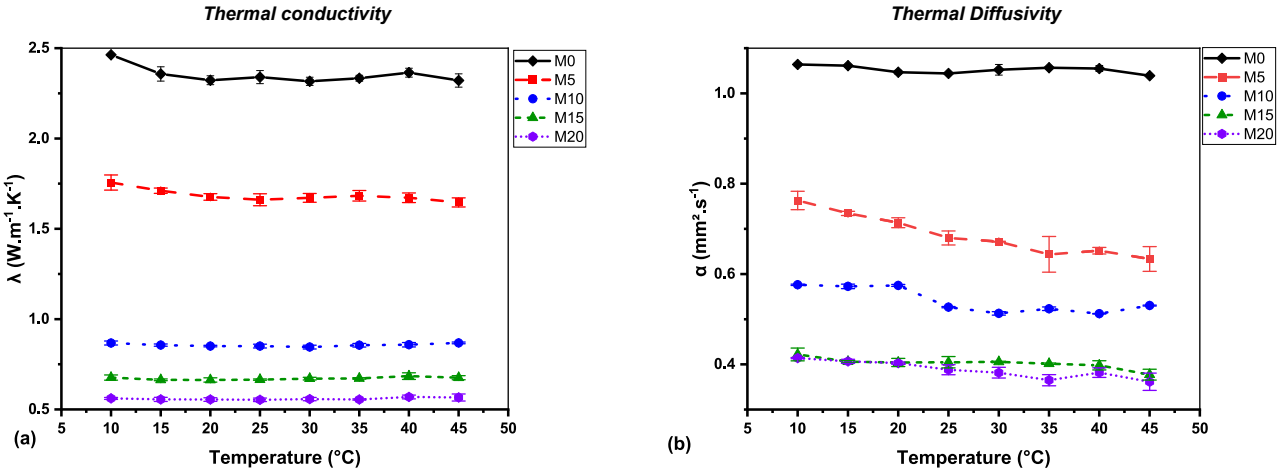

Fig. 19. Evolution of the (a) thermal conductivity and (b) thermal diffusivity with temperature for the various PCM mortars.

experimental data plotted as a function of the volume content of the mPCM particles in the mortar samples.

The M0 reference mortar exhibits high-strength characteristics when compared to conventional cement mortars used in construction. This may be attributed to both the low W/C ratio in this reference mix (0.35) and the characteristics of the sand used in the mix (standard sand with controlled granular distribution and very low moisture content). Notably, the same order of compressive strength was obtained by Khalil *et al.* for M0 mortar [27,28].

Overall, the experimental data highlight significant decreases in both the flexural and compressive strengths of the mortar samples upon the addition of the mPCMs (Fig. 18). Furthermore, the compressive strength was the most affected among the two properties; the addition of 10.5 vol % mPCMs in the mortar (corresponding to ~4.5 wt%) induces a strength reduction of 64 % from 72 to 26.3 MPa.

Although the use of a liquid mPCM dispersion has made it possible to obtain PCM mortars with a homogeneous microstructure (fine mPCM particles uniformly distributed within the cement matrix), a deterioration in the mechanical properties was still observed when compared to the neat mortar. This trend was similar to that reported in the literature for PCM composites prepared using mPCM powders [20–23,45,46]. Indeed, Berardi *et al.* analyzed the results of numerous studies in their review and concluded that the average decrease in the compressive strength of PCM-concrete specimens containing >3 wt% mPCMs was generally >40 % higher than the original value [47]. However, several authors [20,22] have reported mortars with mPCMs contents up to 5 wt % that retain a compressive strength suitable for structural applications.

In the present work, the observed degradation in the mechanical performance of PCM mortars can be explained by several factors, which is in agreement with the conclusions of other authors [20,21,23]: i) mPCM particles exhibit very poor mechanical properties and behave like voids, hence decreasing the mechanical strength of the PCM mortar when compared to neat mortar; ii) the porosity of the mortars increases with the mPCM content due to the excess water added to control the workability and the air entrapped during the mixing process, as shown in the previous sections; iii) the weakness of the bonds between the mPCM particles and the cementitious matrix may also contribute to the loss of strength. Conversely, SEM observations did not reveal any evidence of the breakage of mPCM particles in the PCM mortars and the effect of the leaked PCM on the cement hydration process must be excluded in the present case.

In addition, it is interesting to note that the minimum compressive strength required for structural concrete is 17.2 MPa [47]. Fig. 18 shows that mPCM contents up to ~16 vol% (equivalent to ~8 wt%) may be

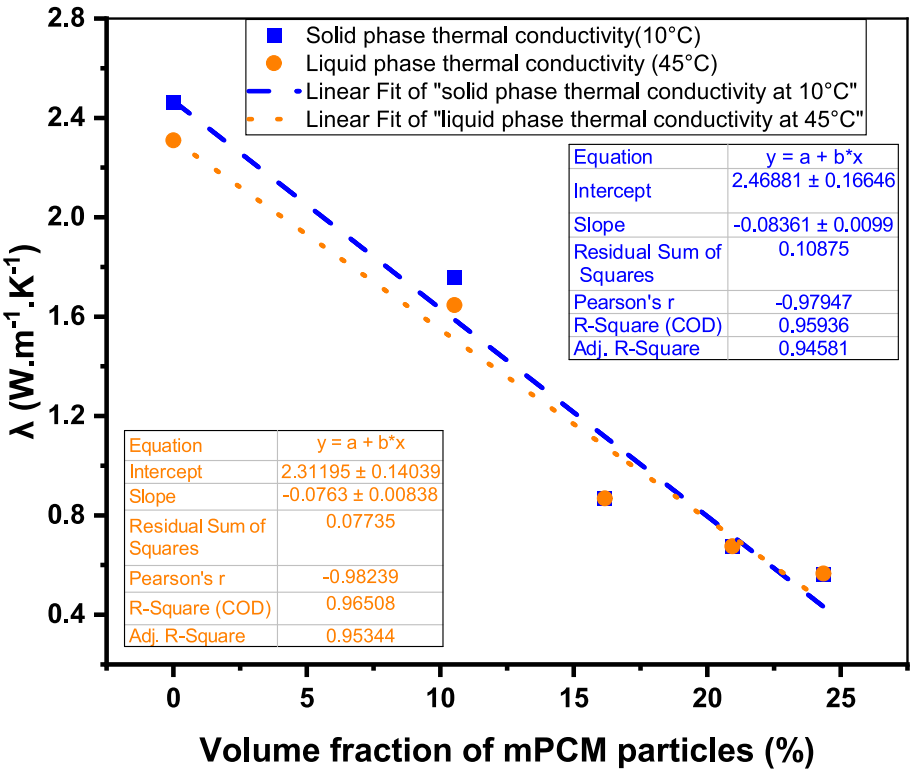

Fig. 20. Evolutions of the thermal conductivity of the PCM mortars as a function of the volume content of mPCM particles in the solid and liquid phase, respectively.

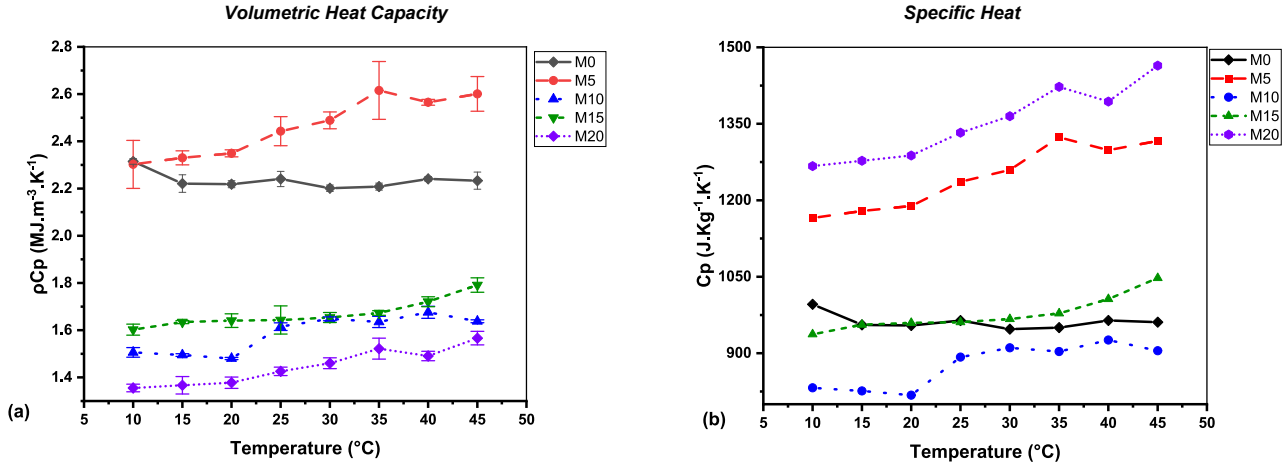

Fig. 21. Evolution of the (a) volumetric heat capacity and (b) specific heat capacity as a function of temperature for the various PCM mortars.

acceptable for structural applications and hence, M0, M5, and M10 are eligible (see details of the mortar compositions in Table 2). In contrast, for higher mPCM contents, the compressive strength of the PCM mortars does not reach the minimum value, and the material should be considered for filling or coating purposes only (M15 and M20).

A possible way to improve the mechanical strength of PCM mortars prepared with liquid mPCM dispersions is to reduce the excess water added during the mixing process. Therefore, the total amount of water may be adjusted to maintain the workability of the mortar mixture (slump) above a minimum level (to be defined), instead of maintaining the workability constant at the level of the reference mortar. This alternative method may provide lower porosity and enhance the mechanical performance of the PCM mortars after 28 d.

3.2.1.5. Thermophysical properties of PCM mortars. The thermophysical properties of the PCM mortars were determined using the hot-disk method according to the protocol detailed in Section 2.3.7. Measurements were performed under a controlled environment at 50 % RH and various temperatures in the range of 10–45 °C to cover the entire domain of the phase transition. In the present study, the experimental values were averaged over three repeated measurements.

Fig. 19a and b present the evolution of the thermal conductivity (λ) and thermal diffusivity (α) for the different PCM mortars as a function of temperature, respectively. The errors bars are also displayed on the graphs based on the standard deviations.

Several studies have shown that the thermophysical properties of regular cement mortars are highly dependent on the density of the material, and to a lower extent, on the moisture content in the samples [48–50]. These studies report typical variation ranges of 1.5–2.7 W m^{-1} K^{-1} for the thermal conductivity, 0.89–1.26 mm^2 s^{-1} for the thermal diffusivity, and 0.87–1.04 KJ Kg^{-1} K^{-1} for the specific heat of the OPC mortars [48]. In addition, Shafigh *et al.* reported λ and α values of 2.4 W

m^{-1} K^{-1} and 1.03 mm^2 s^{-1}, respectively for mortar with a density of 2200 Kg m^{-3} [48]. These findings are in accordance with those obtained in the present work for the reference mortar sample (M0), which has a density in the same order of 2300 Kg m^{-3}; the λ and α values measured at 20 °C were 2.32 W m^{-1} K^{-1} and 1.05 mm^2 s^{-1}, respectively.

Furthermore, the thermal properties of the M0 reference mortar shows little variation in the temperature range of 10 to 45 °C when considering the experimental uncertainties (see Fig. 19), which was also consistent with the literature data [51].

Fig. 19 also shows the substantial decrease in both the thermal conductivity and thermal diffusivity observed upon the introduction of the mPCM particles in the mortar: the curves were roughly shifted downward. When examining the graphs in more detail, it was found that at a given mPCM dosage, both properties slightly decrease in the melting temperature range of the mPCMs (between 20 and 30 °C), and the values in the liquid state (>30 °C) were lower than those in the solid state, especially the thermal diffusivity. This trend was consistent with the variations previously observed for the pure mPCM particles (Fig. 10). All these results confirm that the mPCMs significantly modify the thermal properties of the PCM mortars when compared to the M0 reference material.

Specifically, Fig. 20 shows the evolution of the thermal conductivity of the PCM mortars as a function of the volume content of the mPCM particles. The data obtained at 10 and at 45 °C are plotted in the graphs (at these temperatures, the PCM core was in its solid and liquid states, respectively).

Interestingly, the λvalues decrease almost linearly with the mPCM content (the regression lines enclosed in the graph show that the R^2 coefficients were > 0.95). Such a linear relationship has also been noted by some other authors for PCM mortars prepared with mPCM powders [20,21,45]. In addition, the experimental data measured in the liquid state at 45 °C were slightly lower than those in the solid state, although the difference was very limited. This point remains controversial in the literature because some authors have reported slightly higher thermal conductivities for PCM mortars in the solid state [21], whereas others observed higher values in the liquid state [20,52].

From a quantitative point of view, Fig. 20 shows that the addition of 10.5 vol% mPCMs in the mortar (equivalent to 4.5 wt%) leads to a ~ 29 % decrease in the thermal conductivity (from 2.46 to 1.75 W m^{-1} K^{-1}). This was consistent with the previous studies conducted by Dehdezi *et al.* [46], Hunger *et al.* [22], and Jayalath *et al.* [45], which report reductions in thermal conductivity of ~ 36, ~38, and ~ 45 % upon the addition of 5 wt% mPCMs into the cement composites when compared to the reference specimens. Furthermore, in the present work the PCM mortar with the highest particle content, i.e., M20, including 24.3 vol% of mPCMs (equivalent to 13.6 wt%), shows a very significant decrease in the thermal conductivity (~77 %) with respect to the neat mortar. Hence, mortars with high mPCM contents may be very suitable for insulation applications.

The decreasing trend in the thermal conductivity/diffusivity of mortars with the mPCM content can be mainly attriubted to i) the low conductivity of mPCMs when compared to that of the replaced mineral components and ii) the increased porosity caused by the volume of air entrapped during the incorporation of the mPCM particles [13,21,22,45,46].

Finally, the evolution of the volumetric heat capacity ($\rho.C_p$) of the various PCM mortars as a function of temperature was plotted, as shown in Fig. 21a, and the evolution of the specific heat capacity (C_p) is shown in Fig. 21b (the C_p values were calculated by dividing the volumetric heat capacities by the apparent densities of the PCM mortars previously determined in Section 3.2.1.3).

Overall, the volumetric heat capacity of the mortar samples tends to decrease upon the addition of the mPCMs as the curves shift downward (except for mortar M5). This can be mainly attributed to the decreasing density of the mortars upon increasing the mPCM dosage [22]. In addition, the $\rho.C_p$ value seems to be slightly higher in the liquid state than in the solid state for a given mortar formulation, which was in agreement with the behavior observed for the pure mPCM particles presented in Section 3.1.2.

The decrease in the $\rho.C_p$ values of the PCM mortars compared to the reference material does not support the conclusions of other authors who reported significant improvements in the thermal mass of mortars upon the addition of mPCMs based on DSC measurements [20,22,45]. According to these authors, such an improvement was mainly effective in the temperature range of the phase change transition, where the peak of the thermal mass was observed for the PCM mortars. This effect was not observed in this study, as shown in Fig. 21. However, the $\rho.C_p$ values provided by the HD technique in the melting temperature range should be considered with caution because the system is not in a steady-state and the HD apparatus was pushed to its limits. Therefore, no clear conclusions can be drawn from the present measurements.

4. Conclusions

In this study, the mechanical and thermophysical properties of cement mortars with different dosages of mPCMs are investigated. The major innovations of this work rely on the use of a liquid dispersion of fine mPCM particles instead of the usual dry powders of agglomerated mPCM particles, and the fact that this product is 100 % bio-based, which makes it suitable for the development of TES systems with a reduced environmental footprint.

In the first part of this study, a specific protocol was proposed for the fabrication of mortar samples with a high mPCM content. The liquid mPCM dispersion was incorporated at an early stage of the mixing process, and the total amount of water was adjusted to maintain the constant workability of the fresh mortar mix (as evaluated by slump tests). In general, the water demand increased significantly with the addition of the mPCMs.

Microstructural characterization studies were performed on the various hardened PCM mortars. SEM showed that the mPCM particles were finely and homogeneously distributed in the material, and no signs of breakage/leakage of the mPCM particles were detected. The addition of mPCMs resulted in the lower density and increased water accessible porosity of the mortars, which can be attributed to both the excess water used to control the workability and the air entrapped during the mixing process. Finally, TGA also indicated the variation in the cement hydrate composition of the PCM mortars.

The mechanical properties of the cement mortars were also strongly affected by the introduction of the mPCMs. A loss of compressive strength of ~64 % was observed upon the addition of only 10.5 vol% mPCMs (equivalent to ~4.6 wt%). The PCM mortars retain the minimum strength required for structural applications as long as their mPCM content is <16.2 vol% (equivalent to ~8 wt%).

Conversely, the thermal resistance of the cement mortars was significantly improved upon the addition of the mPCMs. For instance, a decrease in the thermal conductivity of ~77 % was obtained for M20 mortar, including 24.3 vol% mPCM particles (equivalent to ~13.6 wt%). This effect may result from both the intrinsic thermal properties of the mPCMs and the higher porosity of the PCM mortars compared with the M0 reference mortar. However, the HD measurements did not show any improvement in the thermal mass of the PCM mortars with respect to the reference, but these results should be considered with caution because of the limitation in the technique in the temperature range of the phase transition.

Finally, the M10 mortar composition, including ~16.2 vol% mPCMs (equivalent to ~8 wt%), offered an interesting balance between

mechanical and thermal properties. In contrast, mortars with higher amounts of mPCMs should be considered as filling or coating materials without structural function.

As a final remark, the thermal performance of PCM mortars should also be investigated on a wall scale to collect data that are more representative of actual building applications.

CRediT authorship contribution statement

Franck Komi Gbekou: Formal analysis, Methodology, Visualization, Writing – original draft, Writing – review & editing. **Karim Benzarti:** Conceptualization, Formal analysis, Funding acquisition, Methodology, Supervision, Visualization, Writing – original draft, Writing – review & editing. **Abderrahim Boudenne:** Conceptualization, Formal analysis, Methodology, Supervision, Visualization, Writing – original draft, Writing – review & editing. **Anissa Eddhahak:** Formal analysis, Methodology, Supervision, Writing – review & editing. **Myriam Duc:** Formal analysis, Methodology.

Declaration of Competing Interest

The authors declare that they have no known competing financial interests or personal relationships that could have appeared to influence the work reported in this paper.

Data availability

Data will be made available on request.

Acknowledgments

The authors acknowledge the Vicat Company for providing the OPC and Alpenat cements used in this study. They are also very grateful to Dr. Mickael Saillio and Julien Vincent for their help with the TGA experiments performed at the Gustave Eiffel University.

Author Contributions

This research article is based on the Ph.D. work of the first author (K.G). The methodology was proposed and validated by K.G, K.B, A.B, and A.E; K.G, K.B, and A.B participated in conducting the experimental tests. The original draft was prepared by the first author (K.G) and reviewed and edited by K.B, A.B, A.E, and M.D. All authors have read and agreed to the published version of the manuscript.

Funding

This research received financial support from the Labex MMCD (Multiscale Modelling & Experimentation of Materials for Sustainable Construction) through the ANR Investments for the future program (ANR-11-LABX-022-01).

Appendix A:. Complementary tables

Table A1. Table A2.

Table A1
Densities of the raw materials used in the PCM mortar formulations provided by the suppliers.

Component	Standard sand	OPC	CSA	SP	Liquid mPCM dispersion (ME29D)	Solid mPCM particles
Density (Kg m^{-3})	2640	3190	2970	1060	940 (at 25 °C)	870 (at 25 °C)

Table A2
Theoretical compositions of various PCM mortars reported in kg per m^3 for the fresh mix. The W/C ratios and mass and volume fractions of mPCM particles are also reported (they are similar to those previously reported in Table 2).

Designation	Sand	OPC	CSA	SP	Solid mPCM particles	Total amount of water	W/C ratio	Mass fraction of mPCM particles (wt.%)	Volume fraction of mPCM particles (vol.%)
M0	1061.53	832.97	62.69	2.33	0	313.48	0.35	0	0
M5	856.01	671.70	50.56	1.88	91.64370157	341.06	0.47 (+34 %)	4.55	10.53
M10	656.39	515.06	38.77	1.44	140.5501267	413.94	0.75 (+114 %)	7.96	16.16
M15	567.92	445.64	33.54	1.25	182.1815236	423.31	0.88 (+151 %)	11.03	20.94
M20	494.81	388.27	29.22	1.08	211.9026502	436.43	1.05 (+200 %)	13.57	24.35

References

[1] Global Alliance for Buildings and constructions, 2021 Global Status Report for Buildings and Construction, 2021.

[2] International Energy Agency (IEA), Tracking Buildings 2021, Paris, 2021. https://www.iea.org/reports/tracking-buildings-2021.

[3] H. Monteiro, J.E. Fernández, F. Freire, Comparative life-cycle energy analysis of a new and an existing house: the significance of occupant's habits, building systems and embodied energy, Sustain. Cities Soc. 26 (2016) 507–518, https://doi.org/10.1016/j.scs.2016.06.002.

[4] J.S. Carlos, H. Corvacho, P.D. Silva, J.P. Castro-Gomes, Real climate experimental study of two double window systems with preheating of ventilation air, Energy Build. 42 (2010) 928–934, https://doi.org/10.1016/j.enbuild.2010.01.003.

[5] L. Pires, P.D. Silva, J.P. Castro Gomes, Experimental study of an innovative element for passive cooling of buildings, Sustain. Energy Technol. Assess. 4 (2013) 29–35, https://doi.org/10.1016/j.seta.2013.08.002.

[6] L. Pires, P.D. Silva, L.C. Gonçalves, Surface configuration relevance in the overall thermal resistance of a wall, Energy Build. 37 (2005) 1068–1074, https://doi.org/10.1016/j.enbuild.2004.12.012.

[7] I. Sarbu, C. Sebarchievici, A comprehensive review of thermal energy storage, Sustainability 10 (2018) 191, https://doi.org/10.3390/su10010191.

[8] B. Zalba, J.M. Marín, L.F. Cabeza, H. Mehling, Free-cooling of buildings with phase change materials, Int. J. Refrig. 27 (8) (2004) 839–849.

[9] V.A.A. Raj, R. Velraj, Review on free cooling of buildings using phase change materials, Renew. Sustain. Energy Rev. 14 (2010) 2819–2829, https://doi.org/10.1016/j.rser.2010.07.004.

[10] L.F. Cabeza, C. Castellón, M. Nogués, M. Medrano, R. Leppers, O. Zubillaga, Use of microencapsulated PCM in concrete walls for energy savings, Energy Build. 39 (2007) 113–119, https://doi.org/10.1016/j.enbuild.2006.03.030.

[11] A.R. Sakulich, D.P. Bentz, Incorporation of phase change materials in cementitious systems via fine lightweight aggregate, Constr. Build. Mater. 35 (2012) 483–490, https://doi.org/10.1016/j.conbuildmat.2012.04.042.

[12] M. Frigione, M. Lettieri, A. Sarcinella, Phase change materials for energy efficiency in buildings and their use in mortars, Materials 12 (2019) 1260, https://doi.org/10.3390/ma12081260.

[13] M. Fenollera, J. Míguez, I. Goicoechea, J. Lorenzo, M. Ángel Álvarez, The influence of phase change materials on the properties of self-compacting concrete, Materials 6 (2013) 3530–3546, https://doi.org/10.3390/ma6083530.

[14] S.E. Kalnæs, B.P. Jelle, Phase change materials and products for building applications: a state-of-the-art review and future research opportunities, Energy Build. 94 (2015) 150–176, https://doi.org/10.1016/j.enbuild.2015.02.023.

[15] A. Sharma, V.V. Tyagi, C.R. Chen, D. Buddhi, Review on thermal energy storage with phase change materials and applications, Renew. Sustain. Energy Rev. 13 (2009) 318–345, https://doi.org/10.1016/j.rser.2007.10.005.

[16] A. Eddhahak-Ouni, S. Drissi, J. Colin, J. Neji, S. Care, Experimental and multi-scale analysis of the thermal properties of Portland cement concretes embedded with microencapsulated Phase Change Materials (PCMs), Appl. Therm. Eng. 64 (2014) 32–39, https://doi.org/10.1016/j.applthermaleng.2013.11.050.

[17] D. Snoeck, B. Priem, P. Dubruel, N. De Belie, Encapsulated Phase-Change Materials as additives in cementitious materials to promote thermal comfort in concrete constructions, Mater Struct. 49 (2016) 225–239, https://doi.org/10.1617/s11527-014-0490-5.

[18] R. Parameshwaran, R. Naresh, V.V. Ram, P.V. Srinivas, Microencapsulated bio-based phase change material-micro concrete composite for thermal energy storage, J. Build. Eng. 39 (2021), 102247, https://doi.org/10.1016/j.jobe.2021.102247.

[19] CrodaTherm™, Phase change materials, (n.d.). https://www.crodaenergytechnologies.com/en-gb/brands/crodatherm.

[20] T. Lecompte, P. Le Bideau, P. Glouannec, D. Nortershauser, S. Le Masson, Mechanical and thermo-physical behaviour of concretes and mortars containing phase change material, Energy Build. 94 (2015) 52–60, https://doi.org/10.1016/j.enbuild.2015.02.044.

[21] V.D. Cao, S. Pilehvar, C. Salas-Bringas, A.M. Szczotok, J.F. Rodriguez, M. Carmona, N. Al-Manasir, A.-L. Kjøniksen, Microencapsulated phase change materials for enhancing the thermal performance of Portland cement concrete and geopolymer concrete for passive building applications, Energy Convers. Manage. 133 (2017) 56–66, https://doi.org/10.1016/j.enconman.2016.11.061.

[22] M. Hunger, A.G. Entrop, I. Mandilaras, H.J.H. Brouwers, M. Founti, The behavior of self-compacting concrete containing micro-encapsulated Phase Change Materials, Cem. Concr. Compos. 31 (2009) 731–743, https://doi.org/10.1016/j.cemconcomp.2009.08.002.

[23] Z.I. Djamai, F. Salvatore, A. Si Larbi, G. Cai, M. El Mankibi, Multiphysics analysis of effects of encapsulated phase change materials (PCMs) in cement mortars, Cem. Concr. Res. 119 (2019) 51–63, https://doi.org/10.1016/j.cemconres.2019.02.002.

[24] S. Drissi, K.H. Mo, A.C. Falchetto, T.-C. Ling, Understanding the compressive strength degradation mechanism of cement-paste incorporating phase change material, Cem. Concr. Compos. 124 (2021), 104249, https://doi.org/10.1016/j.cemconcomp.2021.104249.

[25] H.R. Dungworth, M. Auerbach, J. Gonthier, E. Parks, Microcapsules, International Patent, WO2017178297A1, WO2017178297A1, 2017. https://patentimages.storage.googleapis.com/e2/d9/50/058b5ec4b9d431/WO2017178297A1.pdf.

[26] CrodaTherm™, CrodaTherm™ ME29D: Microencapsulated ambient temperature phase change material, technical datasheet., (2018). https://www.crodaenergytechnologies.com/en-gb/product-finder/product/1381-CrodaTherm_1_ME29D.

[27] [27] N. Khalil, Formulation et caractérisation chimique et rhéologique des mortiers imprimables en 3D à base de mélanges de ciments Portland et sulfoalumineux, Université de Lille, 2018. https://tel.archives-ouvertes.fr/tel-02900865/document.

[28] N. Khalil, G. Aouad, K. El Cheikh, S. Rémond, Use of calcium sulfoaluminate cements for setting control of 3D-printing mortars, Constr. Build. Mater. 157 (2017) 382–391, https://doi.org/10.1016/j.conbuildmat.2017.09.109.

[29] European Committee for Standardization (CEN), NF EN 196-1: Methods of testing cement — Part 1: Determination of strength, (2016).

[30] S.G. Sanfelix, I. Santacruz, A.M. Szczotok, L.M.O. Belloc, A.G. De la Torre, A.-L. Kjøniksen, Effect of microencapsulated phase change materials on the flow behavior of cement composites, Constr. Build. Mater. 202 (2019) 353–362, https://doi.org/10.1016/j.conbuildmat.2018.12.215.

[31] E37 Committee, Standard Test Method for Determining Specific Heat Capacity by Sinusoidal Modulated Temperature Differential Scanning Calorimetry, ASTM International, n.d. 10.1520/E2716-09R14.

[32] R.B. Cassel, T. Instruments, L. Drive, How Tzero™ Technology Improves DSC Performance Part III: The Measurement of Specific Heat Capacity, (n.d.) 4.

[33] S. Drissi, A. Eddhahak, S. Caré, J. Neji, Thermal analysis by DSC of phase change materials, study of the damage effect, J. Build. Eng. 1 (2015) 13–19, https://doi.org/10.1016/j.jobe.2015.01.001.

[34] TA instruments, Heat Capacity Measurements Using Modulated DSC (MDSC) – Both Ramping and Quasi-isothermal Methods, Application note TA432., (n.d.). https://www.tainstruments.com/pdf/literature/TA432.pdf (accessed January 12, 2022).

[35] AFNOR Editions, NF P18-459, Béton - Essai pour béton durci - Essai de porosité et de masse volumique, (2010).

[36] European Committee for Standardization (CEN), NF EN ISO 22007-2, Plastics — Determination of thermal conductivity and thermal diffusivity — Part 2: Transient planeheat source (hot disc) method, (2015).

[37] Technical specifications of the TPS 2500 S instrument Available online: https://www.hotdiskinstruments.com/products-services/instruments/tps-2500-s/, (n.d.). https://www.hotdiskinstruments.com/products-services/instruments/tps-2500-s/.

[38] S. Kahwaji, M.B. Johnson, A.C. Kheirabadi, D. Groulx, M.A. White, A comprehensive study of properties of paraffin phase change materials for solar thermal energy storage and thermal management applications, Energy 162 (2018) 1169–1182, https://doi.org/10.1016/j.energy.2018.08.068.

[39] M. Aguayo, S. Das, A. Maroli, N. Kabay, J.C.E. Mertens, S.D. Rajan, G. Sant, N. Chawla, N. Neithalath, The influence of microencapsulated phase change material (PCM) characteristics on the microstructure and strength of cementitious composites: experiments and finite element simulations, Cem. Concr. Compos. 73 (2016) 29–41, https://doi.org/10.1016/j.cemconcomp.2016.06.018.

[40] H. Inaba, P. Tu, Evaluation of thermophysical characteristics on shape-stabilized paraffin as a solid-liquid phase change material, Heat Mass Transf. 32 (1997) 307–312, https://doi.org/10.1007/s002310050126.

[41] C. Vélez, M. Khayet, J.M. Ortiz de Zárate, Temperature-dependent thermal properties of solid/liquid phase change even-numbered n-alkanes: n-Hexadecane, n-octadecane and n-eicosane, Appl. Energy 143 (2015) 383–394, https://doi.org/10.1016/j.apenergy.2015.01.054.

[42] N. Essid, A. Loulizi, J. Neji, Compressive strength and hygric properties of concretes incorporating microencapsulated phase change material, Constr. Build. Mater. 222 (2019) 254–262, https://doi.org/10.1016/j.conbuildmat.2019.06.156.

[43] B. Sharma, Incorporation of Phase Change Materials into Cementitious Systems, Azizona State University, 2013.

[44] S. Cunha, J. Aguiar, V. Ferreira, A. Tadeu, Mortars based in different binders with incorporation of phase-change materials: physical and mechanical properties, Eur. J. Environ. Civ. Eng. 19 (2015) 1216–1233, https://doi.org/10.1080/19648189.2015.1008651.

[45] A. Jayalath, R. San Nicolas, M. Sofi, R. Shanks, T. Ngo, L. Aye, P. Mendis, Properties of cementitious mortar and concrete containing micro-encapsulated phase change materials, Constr. Build. Mater. 120 (2016) 408–417, https://doi.org/10.1016/j.conbuildmat.2016.05.116.

[46] P.K. Dehdezi, M.R. Hall, A.R. Dawson, S.P. Casey, Thermal, mechanical and microstructural analysis of concrete containing microencapsulated phase change materials, Int. J. Pavement Eng. 14 (2013) 449–462, https://doi.org/10.1080/10298436.2012.716837.

[47] U. Berardi, A.A. Gallardo, Properties of concretes enhanced with phase change materials for building applications, Energy Build. 199 (2019) 402–414, https://doi.org/10.1016/j.enbuild.2019.07.014.

[48] P. Shafigh, I. Asadi, A.R. Akhiani, N.B. Mahyuddin, M. Hashemi, Thermal properties of cement mortar with different mix proportions, Materiales de Construcción 70 (2020) 224, https://doi.org/10.3989/mc.2020.09219.

[49] A. Stolarska, J. Strzałkowski, The thermal parameters of mortars based on different cement type and W/C ratios, Materials 13 (2020) 4258, https://doi.org/10.3390/ma13194258.

[50] A. Siwińska, H. Garbalińska, Thermal conductivity coefficient of cement-based mortars as air relative humidity function, Heat Mass Transfer. 47 (2011) 1077–1087, https://doi.org/10.1007/s00231-011-0772-1.

[51] M. Pomianowski, P. Heiselberg, R.L. Jensen, Full-scale investigation of the dynamic heat storage of concrete decks with PCM and enhanced heat transfer surface area, Energy Build. 59 (2013) 287–300, https://doi.org/10.1016/j.enbuild.2012.12.013.

[52] F. Alassaad, K. Touati, D. Levacher, N. Sebaibi, Impact of phase change materials on lightened earth hygroscopic, thermal and mechanical properties, J. Build. Eng. 41 (2021), 102417, https://doi.org/10.1016/j.jobe.2021.102417.